THE JOURNAL OF
PHYSICAL CHEMISTRY A

Article

pubs.acs.org/JPCA

Evaluated Kinetics of the Reactions of H and CH_3 with *n*-Alkanes: Experiments with *n*-Butane and a Combustion Model Reaction Network Analysis

Jeffrey A. Manion,* David A. Sheen, and Iftikhar A. Awan

Chemical Sciences Division, National Institute of Standards and Technology, Gaithersburg, Maryland 20899-8320, United States

Supporting Information

ABSTRACT: Presented is a combined experimental and modeling study of the kinetics of the reactions of H and CH_3 with *n*-butane, a representative aliphatic fuel. Abstraction of H from *n*-alkane fuels creates alkyl radicals that rapidly decompose at high temperatures to alkenes and daughter radicals. In combustion and pyrolysis, the branching ratio for attack on primary and secondary hydrogens is a key determinant of the initial olefin and radical pool, and results propagate through the chemistry of ignition, combustion, and byproduct formation. Experiments to determine relative and absolute rate constants for attack of H and CH_3 have been carried out in a shock tube between 859 and 1136 K for methyl radicals and 890 to 1146 K for H atoms. Pressures ranged from 140 to 410 kPa. Appropriate precursors are used to thermally generate H and CH_3 in separate experiments under dilute and well-defined conditions. A mathematical design algorithm has been applied to select the optimum experimental conditions. In conjunction with postshock product analyses, a network analysis based on the detailed chemical kinetic combustion model JetSurf 2 has been applied. Polynomial chaos expansion techniques and Monte Carlo methods are used to analyze the data and assess uncertainties. The present results provide the first experimental measurements of the branching ratios for attack of H and CH_3 on primary and secondary hydrogens at temperatures near 1000 K. Results from the literature are reviewed and combined with the present data to generate evaluated rate expressions for attack on *n*-butane covering 300 to 2000 K for H atoms and 400 to 2000 K for methyl radicals. Values for generic *n*-alkanes and related hydrocarbons are also recommended. The present experiments and network analysis further demonstrate that the C−H bond scission channels in butyl radicals are an order of magnitude less important than currently indicated by JetSurf 2. Updated rate expressions for butyl radical fragmentation reactions are provided.

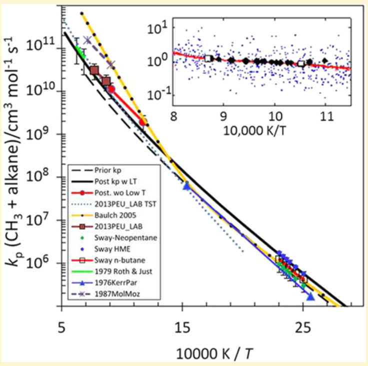

1. INTRODUCTION

A key reaction in both the pyrolysis and combustion of hydrocarbons is the attack of active radicals on the closed shell substrate. The present paper is concerned with the kinetics of the reactions of methyl radicals and hydrogen atoms with *n*-butane, a representative aliphatic fuel. The initial process in both cases is abstraction of H, forming alkyl radicals and either CH_4 or H_2. At high temperatures, the alkyl radicals are unstable, leading to fuel breakdown and propagation of radical chain reactions. Attack of H or CH_3 may occur at either primary or secondary hydrogen sites, however, leading to different subsequent products and chemistry. The relative and absolute rates of these processes are important parameters in combustion and fuel pyrolysis models and can impact global phenomena of interest, such as flame speeds and ignition delay times.

Although these processes have been investigated for many years, there are relatively few data at temperatures near 1000 K. Particularly lacking are results on the branching ratio for attack at the primary and secondary sites. Current recommended values[1−3] are based on extrapolation of sparse lower temperature results or inferred on the basis of complex global phenomena and various assumptions. There are no direct measurements at the temperatures of the present studies, and one of our aims was to fill this informational gap. A difficulty with experimental studies of these reactions at high temperatures is that rapid decomposition of the intermediate alkyl radicals results in the regeneration of both additional H and additional CH_3. Both species can propagate subsequent chains, making it difficult to separate the kinetic behavior under many conditions.

In the present work, we seek to deconvolve the kinetic processes by carrying out a combined set of experiments, wherein H and CH_3 are generated separately in shock-tube experiments in the presence of excess *n*-butane. While both radicals are produced in each system as the chemistry progresses, the intent is to significantly change the contributions of the attacking radicals under the conditions examined.

Special Issue: 100 Years of Combustion Kinetics at Argonne: A Festschrift for Lawrence B. Harding, Joe V. Michael, and Albert F. Wagner

Received: January 30, 2015
Revised: April 9, 2015
Published: April 14, 2015

DOI: 10.1021/acs.jpca.5b01004
J. Phys. Chem. A 2015, 119, 7637−7658

Unlike experiments that probe global phenomena, the systems studied are designed to be well-characterized with limited chemical complexity. The basis of our work is to use short timescales and dilute conditions where there exists a direct correspondence between specific radical intermediates and stable products. This provides a rather direct measurement of the quantities of interest. An experimental design algorithm, recently detailed in a separate article,[4] is applied in conjunction with JetSurf 2,[3] a pre-existing and commonly used combustion model, to select concentrations and conditions that allow the kinetic processes of interest to be disentangled. The results are analyzed on the basis of a detailed chemical kinetic model and polynomial chaos expansion techniques in order to obtain relative and absolute rate constants for attack of H and CH_3 on the primary and secondary hydrogens of *n*-butane.

In our investigation, we compare results when considering only the data obtained from the present experiments near 1000 K and when including reported data from lower temperature studies that have been reviewed herein. The latter analysis leads to evaluated rate expressions for attack of H and CH_3 on the primary and secondary sites of *n*-butane from near ambient to combustion temperatures. On the basis of thermochemical kinetics, and previous work, the expectation is that these rate expressions should be transferrable to related compounds on a per H basis with minimal error and thus serve as generic standard reference values for other aliphatic hydrocarbons. The present experimental product data were also found to constrain the relative rates of C−C and C−H bond scission reactions in butyl radicals, and the experimental results were found to differ from the JetSurF 2 predictions by about an order of magnitude.

2. EXPERIMENTAL METHODS

Shock Tube Methodology. Experiments are carried out in a heated single pulse shock tube configured so as to have reaction times of (500 ± 50) μs, as determined by high-speed pressure transducers. Details of the apparatus have been reported elsewhere.[5] The present study involves the creation of small quantities [<50 μL/L (ppm)] of the attacking radicals of interest, either hydrogen atoms or methyl radicals, via the thermal decomposition of an appropriate precursor. The radicals are generated in the presence of much larger concentrations of *n*-butane, the substrate of interest. Attack of the radical on *n*-butane generates intermediate alkyl radicals that subsequently decompose via unimolecular reactions to stable reaction products that are determined in postshock gas chromatographic (GC) analyses. In some, but not all cases, the radical chain inhibitor toluene has been added to the mixtures.

Shock temperatures in our experiments are determined by following a standard unimolecular reaction with well-defined rate parameters. Experimental rate constants are determined utilizing

$$k_{\mathrm{std}} = \tau^{-1} \ln([\mathrm{std}]_i/[\mathrm{std}]_f)$$

where τ is the reaction time and the subscripts i and f refer to the initial and final concentrations, respectively. The rate expression for the standard, $k_{\mathrm{std}} = A\ \exp(-E/T)$, is easily rearranged to obtain the temperature of a particular experiment. The work reported herein uses the unimolecular decompositions of chlorocyclopentane, 4-vinylcyclohexene, and hexamethylethane (HME) as standard reactions, the selection based on the mixture and temperature range of interest. In all cases, the monitored reaction products from the standards are expected to be stable and not formed by any other processes. The rate parameters, taken from previous work,[6,7] including our recent examination of several temperature standards[7] are $k(\text{chlorocyclopentane} \rightarrow \text{cyclopentene} + \text{HCl})/\text{s}^{-1} = 4.47 \times 10^{13} \exp(-24570\ \text{K}/T)$, $k(\text{4-vinylcyclohexene} \rightarrow \text{2butadiene})/\text{s}^{-1} = 2.51 \times 10^{15} \exp(-31100\ \text{K}/T)\ \text{s}^{-1}$, and $k(\text{hexamethylethane} \rightarrow 2\ t\text{-butyl})/\text{s}^{-1} = 2.51 \times 10^{16} \exp(-34400\ \text{K}/T)\ \text{s}^{-1}$. For mixtures containing HME, chlorocyclopentane (CCP) was used as the temperature standard below 1030 K. At higher temperatures, where conversion of CCP is nearly complete, it is not an appropriate standard because the small amount of unreacted material in the wall boundary layer is enough to perturb the measured rate constants and, thereby, the derived temperatures.[7] Under these conditions, HME itself was used as the standard. For the above standards and temperature range, standard uncertainties (1σ) in the derived absolute shock temperatures are expected to be about 1%.[6,7]

Generation of CH_3 and H Atoms. In the remainder of this report, we will, for convenience, use reaction numbering that matches the final reaction model as provided in the Supporting Information. Methyl radicals are generated from the thermal decomposition of *tert*-butylperoxide (di-*tert*-butylperoxide, *t*BPO):

$$(tert\text{-}C_4H_9O)_2 \rightarrow 2(CH_3)_3CO \tag{R818}$$

$$(CH_3)_3CO \rightarrow CH_3 + (CH_3)_2C{=}O \tag{R819}$$

The kinetics of R818 were determined by Raley et al.[8] 60 years ago and the process has been extensively studied since. The available rate data[9] are in good agreement. Lewis[10] reported $k/\text{s}^{-1} = 2.14 \times 10^{15} \exp(-18300\ \text{K}/T)$ from studies at (528 to 677) K and a linear extrapolation of these results indicates a half-life of about 0.2 μs at 900 K. Decomposition of the *tert*-butoxy radical, R819, is several orders of magnitude faster,[11−13] with the consequence that under our conditions, *tert*-butylperoxide is completely decomposed and can be considered to be a pulse source of acetone and methyl radicals. The acetone formed stoichiometrically with CH_3 in reaction (R819) is stable and inert under our conditions. It provides a direct count of the number of CH_3 radicals released into the system by the precursor. When compared with total product formation, this provides an indication of chain length and thus an experimental measure of the complexity of any secondary chemistry.

A convenient source of hydrogen atoms is hexamethylethane (HME), which decomposes thermally via

$$\text{hexamethylethane} \rightarrow 2t\text{-butyl} \tag{R817}$$

$$t\text{-butyl} \rightarrow \text{isobutene} + \text{H} \tag{R616}$$

This process has been used in this laboratory for many years. The initial bond fission in HME is the rate-limiting step, with radical decomposition R616 requiring a few microseconds or less under our conditions. Compared with *t*BPO, HME decomposes much more slowly, so that H atoms are not released as an initial pulse but rather are generated over the full shock-heating time period. Analogous to *t*BPO, HME decomposition produces a stable coproduct, isobutene, that provides a direct count of the H atoms released into the system by the precursor. This can again be used to gauge the complexity of the secondary chemistry.

While HME decomposition represents a generally clean source of H atoms, Tsang has reported[14] the formation of propene as a minor side process, corresponding to 3% of isobutene formation. This result has been checked by us in separate experiments with mixtures containing only HME, inhibitor, and argon. We find propene/isobutene product ratios of (0.035 ± 0.007) under our conditions. In our studies with HME, the propene yield attributed to attack on *n*-butane was thus reduced by an amount equal to 0.035[isobutene], resulting in a correction of typically 3% or less.

Gas Chromatographic–Mass Spectral Analyses. Following the shock, samples are extracted via an automated valve and loop system for analysis. The port is located 5 cm from the end wall of the shock tube. The present analyses utilized a Hewlett-Packard 6890N GC equipped with two columns and both flame ionization (FID) and mass spectral (MS) detectors. A Restek 30 m x 0.53 mm i.d. Rt-Alumina (aluminum oxide porous layer) capillary column was utilized for optimized detection of the lighter gases (typically smaller than C5). Larger species were separated on a J & W Scientific 30 m × 0.53 mm i.d. DB-1 (100% dimethypolysiloxane) capillary column. Effluent from the DB-1 column was quantitatively split with an Agilent Technologies microfluidic splitter (Dean's Switch) and simultaneously sent to MS and FID detectors. Concentrations are based on the FID analyses, with the MS used primarily to confirm product identities. Chilled nitrogen gas is used to initially cool the GC oven, and analyses are carried out using a ramped temperature program spanning 213 to 453 K (−60 to 180 °C) with constant carrier gas flow. This allows separation of many of the lighter components on both columns, leading to duplicate analyses of these species. In these cases, results agreed typically within a few percent.

Molar FID responses of all product olefins were determined from standard samples. Including possible systematic errors, we estimate the standard analytical uncertainty (1σ) for the main C1 to C3 products to be about 3%.

Chemicals. *n*-Butane (99+ %, Aldrich), *tert*-butyl-peroxide, (98%, Aldrich), hexamethylethane (98%, Aldrich), chlorocyclopentane (99%, Aldrich), 4-vinylcyclohexene (98%, Aldrich), toluene (99%, Aldrich) and argon (Praxair, 99.999%), were the chemicals used in the kinetic studies. Except for toluene, which was redistilled, all chemicals were used without further purification, other than degassing during preparation of the mixtures. GC analyses of the resulting mixtures revealed only the usual traces of hydrocarbon impurities, none of which were present in quantities expected to impact the results for the major species. Product amounts were corrected for trace backgrounds, if present.

Selection of Experimental Conditions. The particular mixtures and sets of experimental conditions that are examined herein are based on a mathematical design algorithm that we describe more fully elsewhere.[4] In brief, the design algorithm considers a selected set of possible experiments covering a range of pressure, temperature combinations that are accessible with our shock tube, a selection of possible mixture compositions, and the experimental observables. This is the full data set. An existing Prior model of the expected chemistry, presently based on JetSurf 2,[3] is then used to simulate the results and determine how well the full data set constrains the model parameters of interest, in this case, the rate parameters for attack of H and CH_3 on *n*-butane. The algorithm is then applied to generate a minimal data set that spans the rate parameter space as completely as possible while containing the fewest possible redundancies. The selected mixture compositions for the experiments are based on this minimal data set and are given in Table 1.

Table 1. Starting Gas Mixtures Used in the Present Experiments[a]

mix	components in mixtures (μL/L)[b]					
	n-butane	*t*BPO	HME	toluene	CCP[c]	4VCE[c]
(A) *t*BPO	10 712	33.2	–	40 295	53.1	–
(B) *t*BPO	11 316	28.3	–	33 237	–	45.9
(C) HME	1 021	–	57.3	–	33.8	–
(D) HME	1 028	–	59.4	10 223	31.6	–
(E) HME	12 854	–	62.4	15 724	41.6	–
(F) *t*BPO	1 140	29.1	–	17 435	51.7	–
(G) *t*BPO	1 158	28.2	–	16 981	48.2	41.8

[a]The remaining balance is argon. [b]Listed concentrations are the unrounded values used in the simulations and do not imply accuracy. Uncertainties (2σ) in the absolute amounts are estimated as 5%. *t*BPO = *tert*-butylperoxide; HME = hexamethylethane; CCP = chlorocyclopentane; and 4VCE = 4-vinylcyclohexene. [c]Temperature standard.

Note that a radical chain inhibitor in the form of toluene has been added to most mixtures. The general function of the inhibitor is to convert highly active radicals to a relatively unreactive species, the benzyl radical, which then terminates radical chains via radical recombination reactions. This prevents runaway radical chain reactions that would disconnect the observed olefin product spectrum from the reactions of interest. Ideally, one would interrupt the chemistry after a single abstraction/decomposition cycle and observe the product spectrum at that point. Secondary chemistry prevents this, but the inhibitor significantly reduces the chain length and thereby brings one closer to the ideal situation. In the experiments using tBPO (corresponding to methyl radicals), the inhibitor is important to prevent highly active H atoms formed in the secondary chemistry from perturbing the results by attack on butane. The inhibitor in fact converts H atoms back to methyl radicals via the displacement reaction H + toluene → benzene + CH_3. In experiments with HME (corresponding to H atoms), the methyl radicals formed by secondary chemistry have less impact because they are less reactive than H. For this system, the experimental design algorithm suggests an additional experiment without added inhibitor (mixture C). Additional discussion can be found in our previous paper.[4]

3. SHOCK TUBE DATA

Data have been obtained for a large number of product species present in a wide range of concentrations. Representative results are visually summarized in Figure 1, in which product amounts are expressed as molar ratios relative to ethene, one of the main marker species for the title reactions. Our subsequent model provides a quantitative kinetic analysis, but Figure 1 gives some qualitative indications of the importance of various products. Experimental conditions and product data for all mixtures are tabulated in the Supporting Information.

Products and Mechanism: Experiments with *t*-Butylperoxide (*t*BPO). Decomposition of *t*BPO produces an initial pulse of methyl radicals and acetone, the latter of which is observed as a stable byproduct whose amount is independent of temperature and invariant for each mixture. Also unrelated to the chemistry of interest are the decomposition products of our temperature standards, cyclo-

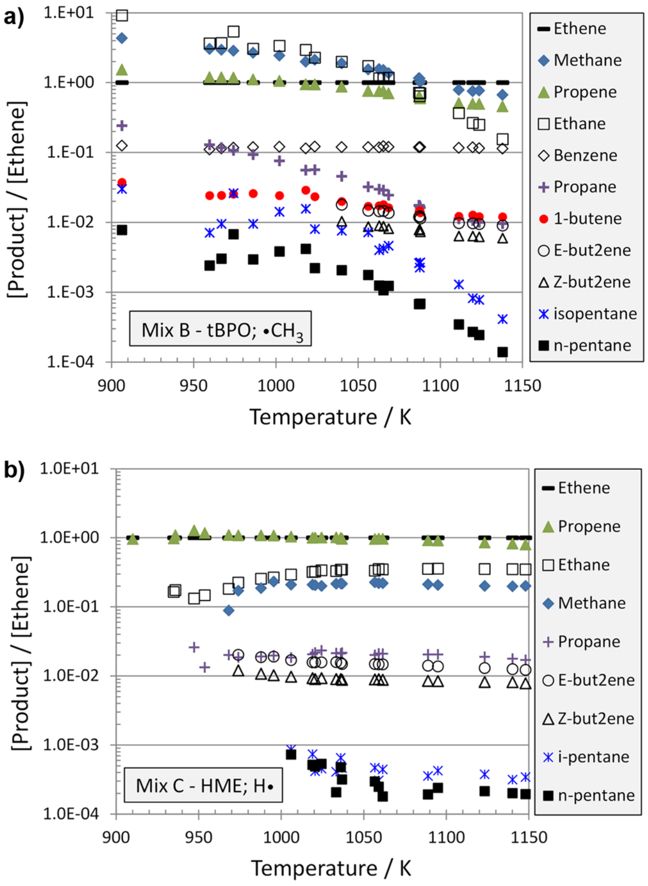

Figure 1. Representative product data from mixture B (methyl radicals, *t*BPO precursor) and mixture C (H atoms, HME precursor), expressed as molar ratios relative to ethene. Results for other mixtures are qualitatively similar. Pressures increase with temperature and are in the range from 150 to 300 kPa.

pentene from chlorocyclopentane (mixture A), and 1,3-butadiene from 4-vinylcyclohexene (mixture B). Other products are attributed as direct or indirect products of the reaction of methyl radicals with the substrate and inhibitor.

The four main products are methane, ethane, ethene, and propene. Several other species are observed at levels corresponding to typically a few percent or less of the main products, including benzene, ethylbenzene, propane, 1-butene, *E*-2-butene, *Z*-2-butene, *n*-pentane, and isopentane.

The major products are accounted for by the following set of reactions:

$$CH_3 + CH_3 \rightarrow C_2H_6 \tag{R107}$$

$$CH_3 + n\text{-butane} \rightarrow \text{1-butyl} + CH_4 \tag{R643}$$

$$CH_3 + n\text{-butane} \rightarrow \text{2-butyl} + CH_4 \tag{R644}$$

$$\text{1-butyl} \rightarrow C_2H_4 + C_2H_5 \tag{R582}$$

$$C_2H_5 \rightarrow C_2H_4 + H \tag{R252}$$

$$\text{2-butyl} \rightarrow C_3H_6 + CH_3 \tag{R592}$$

$$H + n\text{-butane} \rightarrow \text{1-butyl} + H_2 \tag{R633}$$

$$H + n\text{-butane} \rightarrow \text{2-butyl} + H_2 \tag{R634}$$

Note that isomerization reactions of the butyl radical intermediates are not included here. Three and four center H-transfer processes are the only ones that would change the position of the radical center, and these have high barriers. At our temperatures and pressures, experiment[15−18] and theory[19−21] show that such reactions are slow relative to β C−C scissions (a few percent or less) and are therefore unimportant.

Under conditions of excess *n*-butane, consideration of the above reactions makes it apparent that an important factor determining methane to ethane product ratios is the competition between recombination of methyl radicals R107 and abstraction of hydrogen from *n*-butane by CH_3 R643 and R644. At our temperatures, the unimolecular decomposition of C2 and higher alkyl radicals to stable olefins via β-scission reactions requires a few microseconds or less,[15−17] so that under our dilute conditions, the expectation is that this is the dominant process and that competing bimolecular processes are minimal. As a result, there is a direct correspondence between the olefins formed in R582, R592, and R252 and the precursor radicals. Propene to ethene ratios thus reflect the net relative rates of radical attack on the primary and secondary hydrogens of *n*-butane. Notice, however, that both CH_3 and H may play a role, and that these attacking radicals are regenerated by the rapid β-scission reactions R252 and R592. A primary difficulty is in separation of the relative contributions of H and CH_3 in determining the final olefin product spectrum.

Experimentally, a clear indication of the presence of hydrogen atoms in the *t*BPO system (nominally CH_3 radicals) is the formation of benzene, the result of the well-known[22] displacement of methyl from the toluene inhibitor by H atoms:

$$H + \text{toluene} \rightarrow C_6H_6\ (\text{benzene}) + CH_3 \tag{R674}$$

H and CH_3 also attack toluene via abstraction of the methyl hydrogens, leading to the resonance stabilized benzyl radical.

$$H + \text{toluene} \rightarrow C_7H_7\ (\text{benzyl}) + H_2 \tag{R673}$$

$$CH_3 + \text{toluene} \rightarrow C_7H_7\ (\text{benzyl}) + CH_4 \tag{R676}$$

This is of course the mode of action of the inhibitor, replacing active radicals with benzyl radical, a much less reactive species. It also leads to the observed ethylbenzene via recombination with CH_3.

$$CH_3 + \text{benzyl} \rightarrow \text{ethylbenzene} \tag{R805}$$

Plausible routes to the minor C3 to C5 species are put forth below:

$$CH_3 + C_2H_5 \rightarrow C_3H_8\ (\text{propane}) \tag{R279}$$

$$CH_3 + \text{1-butyl} \rightarrow nC_5H_{10}\ (n\text{-pentane}) \tag{R869}$$

$$CH_3 + \text{2-butyl} \rightarrow iC_5H_{10}\ (i\text{-pentane}) \tag{R870}$$

$$\text{2-butyl} \rightarrow E\text{-2-butene} + H \tag{R565a}$$

$$\text{2-butyl} \rightarrow Z\text{-2-butene} + H \tag{R565b}$$

$$\text{1-butyl} \rightarrow \text{1-butene} + H \tag{R553}$$

$$\text{2-butyl} \rightarrow \text{1-butene} + H \tag{R554}$$

Of these, only the recombination reaction of methyl and butyl radicals had to be added to the JetSurf 2 reaction set. Ejection of H from butyl radicals R565a, R565b, R553, and R554 can

DOI: 10.1021/acs.jpca.5b01004
J. Phys. Chem. A 2015, 119, 7637−7658

Table 2. List of Target Values from the Present Experiments Used to Constrain the Model[a]

Measurements using *t*-BPO								
	target values (μL/L)							
T (K)	C_2H_4[b]	C_3H_6[b]	C_2H_6	CH_4	C_3H_8	C_6H_6	1-C_4H_8	2-C_4H_8
Mixture A								
850	1.94	3.16	26.47	9.99	0.60			
950	4.76	5.70	24.60	17.11	0.61	0.72		
1050	9.84	9.19	23.18	26.45	0.61	1.14		
Mixture B								
950	3.83[c]	4.95[c]	22.01	12.94[c]	0.77	0.65[c]	0.11[c]	0.16[c]
1100	50.95	29.23	24.79	49.73[c]	0.82	8.44	0.71[c]	0.93[c]
Mixture F								
850	0.23	0.37	24.18	3.60[c]	0.09	0.37		
950	0.67	0.77	21.93	7.32[c]	0.11	0.53		
1050	1.63	1.38	20.25	13.00[c]	0.12	0.71		
Mixture G								
900	0.38	0.50	22.28	5.36[c]		0.29		
1000	1.04	0.94		9.19[c]				
1100	5.67	2.29	19.78	15.27[c]		2.33		

Measurements using HME						
	target values (μL/L)		target values (dimensionless)			
T (K)	C_2H_4	C_3H_6	C_2H_4/C_3H_6	C_2H_4/C_6H_6	1-C_4H_8/C_3H_6	2-C_4H_8/C_3H_6
Mixture C						
950	0.29[c]	0.32[c]	0.86[d]			
1150	124.0	105.6[c]	1.22[d]			
Mixture D						
950	0.40[c]	0.34[c]	1.09[d]	0.51[d]		
1050					0.032[c]	0.024[c]
1150	22.4[c]	14.9[c]	1.55[d]	0.91[d]	0.046[c]	0.030[c]
Mixture E						
950	0.58[c]	0.66[c]	0.88[d]	5.75[d]		
1050					0.020[c]	0.031[c]
1150	273.1[c]	184.9[c]	1.48[d]	10.70[d]	0.025[c]	0.030[c]

[a] All concentrations and concentration ratios precise to a factor of 1.2 (σ^{obs} = 0.1), unless noted. [b] C_2H_4/C_3H_6 ratio has σ^{obs} = 0.05 (2σ uncertainty factor of 1.1). [c] σ^{obs} = 0.2 (2σ uncertainty factor of 1.5). [d] σ^{obs} = 0.05 (2σ uncertainty factor of 1.1).

lead to the trace butene products that are observed and is less favored than the β C−C scissions R582 and R592. In the present work, the experimentally observed ratios of butene to propene and ethene suggest branching fractions for C−H scission of about 0.03, consistent with our recent observations of related systems.[15,17] As discussed later, the starting JetSurf 2 model significantly overpredicted C−H bond scission channels in butyl radicals, and the relevant rate parameters were adjusted in the course of this work. With the exception of propane formation, R279, which was found to play a role in the *t*BPO system at the lower temperatures of our study, the above minor reactions have minimal impact on observed ethene/propene ratios.

Products and Mechanism: Experiments with HME. Isobutene and cyclopentene are the only measured products not attributed directly or indirectly to reaction of H with the substrate or inhibitor. The former is the olefin produced in R616 from our H atom precursor, and the latter is from our temperature standard. Changing the precursor from *t*BPO to HME results in a different initial radical pool, but the main products are produced by the same set of reactions, and the product spectrum is qualitatively similar to that observed with *t*BPO. Ethene and propene remain the main olefin products. When the inhibitor toluene is present, amounts of benzene are significantly increased relative to the *t*BPO results, an indication of higher concentrations of H atoms in the HME case and a resulting increase in the rate of R674. Conversely, methyl radical concentrations are much lower in the HME system, as indicated by much smaller amounts of the methane and ethane products. These observations are consistent with the expectation that the relative contributions of methyl and H are significantly different in the HME and *t*BPO systems, thus allowing good separation of the kinetics.

4. MODELING METHODS

Method Overview. The above discussion provides a qualitative description of the most important chemistry. As indicated, the data suggest that the relative concentrations of the attacking methyl and H radicals are significantly different in the HME and *t*BPO systems. One could use this observation, together with an abbreviated reaction set and certain simplifying assumptions, to derive analytical expressions with respect to the kinetics of the two species. We believe a better approach, however, is to explicitly include potential secondary chemistry through the use of a detailed reaction model comprised of a larger reaction set, together with uncertainty analysis techniques to analyze the data. The methodology entails the use of an initial reaction model (the Prior model) in which the relevant parameters (rate coefficients) are each assigned a known or assumed uncertainty. The permissible

DOI: 10.1021/acs.jpca.5b01004
J. Phys. Chem. A 2015, 119, 7637−7658

Table 3. List of Literature Rate Constant Measurements and Physico-Chemical Rules Used to Constrain the Posterior Model

Literature Estimates for X + C_4H_{10}					
	H + C_4H_{10}			CH_3 + C_4H_{10}	
T (K)	ln k_s/k_p[a]	reference	T (K)	ln k_s/k_p[a]	
318	3.61 ± 0.4[b]	1969CamStr[48]	371	2.02 ± 0.25	1966TedWat[38]
413	2.88 ± 0.4	1969CamStr[48]	492	1.47 ± 0.25	1966TedWat[38]
			523	1.51 ± 0.25	1956McNGor[37]
			722	1.39 ± 0.25	1956McNGor[37]
			T (K)	ln k_p[ac]	
			399	4.17×10^5 ± 0.6	1990Sway[40]
			434	1.21×10^6 ± 0.6	1990Sway[40]
Constraint of X + C_4H_{10} to X + C_2H_6					
	H + C_2H_6			CH_3 + C_2H_6	
ln A_e/A_p[a]	4.83 ± 0.6		ln A_e/A_p[a]	15.73[c] ± 0.6	
$E_e - E_p$[a]	390 K ± 100 K		$E_e - E_p$[a]	1664 K ± 100 K	
Literature Estimates for X + C_4H_{10}					
	H + C_2H_6			CH_3 + C_2H_6	
T (K)	ln k_e[ac]	reference	T (K)	ln k_e[ac]	reference
400	20.36 ± 0.4	1963Yang[57]	1153	23.57 ± 0.4	2013Peu[41]
513	22.66 ± 0.4	1963Yang[57]	1297	24.15 ± 0.4	2013Peu[41]
467	22.44 ± 0.4	2001BruSla[64]			
826	26.74 ± 0.4	2001BruSla[64]			
544	23.83 ± 0.4	1977JonMor[65]			
385	20.31 ± 0.4	1977JonMor[65]			
298	16.62 ± 0.4	1969AzaFil[67]			
Physico-chemical Reaction Rate Constraints					
Geometric Mean Rules					
A_{mm}[b]		2.12×10^{16}		Rmm: $2CH_3 \leftrightarrow C_2H_6$	
ln A_{mm}/A_{me}		3.77[e] ± 0.2		Rme: $CH_3 + C_2H_5 \leftrightarrow C_3H_8$	
ln A_{mm}/A_{ee}		4.73[e] ± 0.2[d]		Ree: $2C_2H_5 \leftrightarrow C_4H_{10}$	
ln A_{mm}/A_{mb}		−5.95[d] ± 0.2		Rmb: $CH_3 + C_6H_5CH_2 \leftrightarrow C_6H_5C_2H_5$	
ln A_{mm}/A_{bb}		−10.51[d] ± 0.2		Rbb: $2C_6H_5CH_2 \leftrightarrow C_6H_5C_2H_4\ C_6H_5$	
2-Butyl Dissociation					
A_m[b]		1.20×10^4		Rm: $CH_3 + C_3H_6 \leftrightarrow$ s-C_4H_9	
ln A_m/A_h		−9.54 ± 0.02		Rh: H + 1-$C_4H_8 \leftrightarrow$ s-C_4H_9	

[a] Subscript p, s, and e refer to rate parameters for the reactions X + $C_4H_{10} \leftrightarrow$ XH + *p*-C_4H_{10}, X + $C_4H_{10} \leftrightarrow$ XH + *s*-C_4H_{10}, and X + $C_2H_6 \leftrightarrow$ XH + C_2H_5, respectively, where X is H or CH_3. [b] All uncertainties are 2σ; subscripts denote reactions as specified in the subsequent column. [c] All rate constant units are (cm^3/mol s). [d] Ratios of *A* differ from unity because *b* values in the modified Arrhenius expressions differ. See Tables 4 and 5 for Arrhenius expressions and *b* values. [e] Constraint removed due to consistency analysis.

solution space of the Prior model can be defined by carrying out multiple trial runs in which rate parameters are randomly varied within their uncertainties. The present experimental observations, with assigned uncertainties, are then used as the basis for adjustment (conditioning) of the Prior model using the subsequently described formalism. The result is a Posterior model in which certain active rate constants are better determined. More details are provided below.

Prior Reaction Model and Active Parameter Determination. The Prior model is the jet surrogate fuel model, version 2 (JetSurF 2),[3] augmented to include formation of ethylbenzene and thermal decomposition of HME and *t*BPO.[23] It has 356 species and 2190 reactions. Measurements from the current experiments and from the literature that were used to constrain the model are listed in Tables 2 and 3, respectively, and will be discussed in detail later. To reduce the computational costs the optimization considers only a representative selection of experiments covering the range of conditions examined. Uncertainty in the current experimental measurements was estimated by fitting a modified Arrhenius equation to the experimental data and calculating the uncertainty in the regression. This gives a 1σ uncertainty of approximately 0.05−0.1, equivalent to a 2σ uncertainty 10−20%. Target values at the nominal temperatures given in Table 2 are computed from these fits. Active parameters are selected by a one-at-a-time sensitivity analysis. For each measurement r and reaction rate parameter i (either an Arrhenius prefactor or activation energy), the uncertainty-weighted sensitivity coefficient $\mathcal{S}_{r,i}$ was computed,

$$\mathcal{S}_{r,i} = \frac{d\eta_r}{d\theta_i}\frac{\theta_i}{\eta_r}\ln f_i \tag{1}$$

where η_r is the simulation-predicted value of measurement r, θ_i is the generalized rate parameter, and f_i is its uncertainty factor. The active rate parameters were selected as those for which $\mathcal{S}_{r,i}/\mathcal{S}_{r,\max} > 0.02$. Uncertainty factors in the Arrhenius prefactors are taken from JetSurF 2[3]. Uncertainty factors in activation energies were estimated using $f_i = (E_k + T_c \ln F_k)/E_k$, where E_k is the activation energy of reaction R_k, and F_k is the uncertainty in the Arrhenius prefactor of reaction R_k, with T_c = 1000 K. This formulation ensures that the activation energy contributes the same uncertainty to the rate constant as the Arrhenius prefactor at 1000 K. If the activation energy is small relative to T_c and the uncertainty factor derived by this method is greater than 1.2, it is capped at 1.2. In simulations, the shock tube was treated as a homogeneous adiabatic reactor. Species concentrations following the shock were determined using the VODE solver[24] to integrate the chemical rate equations supplied by Sandia CHEMKIN[25] over a period of 500 μs.

Model Constraint and Uncertainty Minimization. Model constraint uses the method of uncertainty analysis using polynomial chaos expansions (MUM-PCE),[26] which is summarized here. In this method, a Prior model is defined, which in this case is JetSurF 2. This model is then conditioned on the set of experimental measurements to produce the best Posterior model given the Prior model and experimental data. MUM-PCE assumes that the uncertain parameters in the model can be expressed as a random vector $\mathbf{X} = \mathbf{x}^{(0)} + \mathbf{x}^{(1)}\boldsymbol{\xi}$, where $\mathbf{x}^{(0)}$ is the reduced variable vector whose elements are

$$x_i^{(0)} = \frac{\ln \theta_i/\theta_{i,0}}{\ln f_i} \tag{2}$$

where f_i is the uncertainty factor of the ith active parameter θ_i, which has a nominal value of $\theta_{i,0}$. $\boldsymbol{\xi}$ is a vector of independent, identically distributed normal random variables with mean 0 and variance 1, and $\mathbf{x}^{(1)}$ is a transformation matrix, so that $\mathbf{X}$ follows a multivariate normal distribution with mean $\mathbf{x}^{(0)}$ and covariance matrix $\sum = \mathbf{x}^{(1)}\mathbf{x}^{(1)^T}$.

MUM-PCE applies Bayes' Theorem to determine the joint probability density function (PDF) of the active parameters, which results in the following PDF for the rate parameters in the Posterior model

$$\ln P_{\mathbf{X}}(\mathbf{x}) \sim -\left[\sum_{r=1}^{N_e}\left(\frac{\eta_r(\mathbf{x}) - \eta_r^{\text{obs}}}{\sigma_r^{\text{obs}}}\right)^2 + \sum_{N_r}^{i=1} 4x_i^2\right] \tag{3}$$

where $\eta_r(\mathbf{x})$ is the model prediction as a function of the factorial variables $\mathbf{x}$, N_e is the number of experiments, and N_r the number of active variables. η_r^{obs} is the corresponding measured value, and σ_r^{obs} is its observed uncertainty. This PDF can be approximated by a multivariate normal distribution, which will then have an optimized parameter vector $\mathbf{x}^{(0)*}$ that best reproduces the experimental measurements, and a covariance matrix $\sum^*$ that best reproduces their uncertainty. $\mathbf{x}^{(0)*}$ is found by solving the least-squares optimization problem

$$\mathbf{x}^{(0)*} = \underset{\mathbf{x}}{\text{argmax}} \ln P_{\mathbf{X}}(\mathbf{x}) \tag{4}$$

which is solved using the LMDIF solver in the MINPACK library.[27] $\sum^*$ is found by linearizing the model predictions in the vicinity of $\mathbf{x}^{(0)*}$, which yields

$$\Sigma^* = \left(\sum_{r=1}^{N_e}\frac{\mathbf{J}_r\mathbf{J}_r^T}{(\sigma_r^{\text{obs}})^2} + 4\mathbf{I}\right)^{-1} \tag{5}$$

where $\mathbf{J}_r$ is the gradient of $\eta_r(\mathbf{x}^{(0)*})$, which is then found by taking the Cholesky factorization of $\sum^*$. To reduce the computational complexity of solving eqs 4 and 5, the method of solution mapping[28,29] is used, in which predicted values of experimental measurements are expressed as polynomials with respect to the reaction rate parameters, $\eta_r(\mathbf{X}) = \mathbf{X}^T\mathbf{b}_r\mathbf{X} + \mathbf{a}_r^T\mathbf{X} + \eta_0$, where $\mathbf{a}_r$ and $\mathbf{b}_r$ are the first and second derivatives of η_r. Then $\mathbf{J}_r$ in eq 5 is $\mathbf{J}_r = 2\mathbf{b}_r\mathbf{x}^{(0)*} + \mathbf{a}_r$.

Once the optimized model has been determined, uncertainty in any of the simulations can be calculated by propagating the values of $\mathbf{x}^{(0)*}$ and $\mathbf{x}^{(1)*}$ into the solution mapping polynomial [i.e., $\eta_r(\xi) = \xi^T\hat{\beta}_r\xi + \hat{\alpha}_r^T\xi + \eta_r(\mathbf{x}^{(0)*})$], where $\hat{\beta}_r = \mathbf{x}^{(1)*^T}\mathbf{b}_r\mathbf{x}^{(1)*}$ and $\hat{\alpha}_r = \mathbf{x}^{(1)*^T}\mathbf{J}_r$. The uncertainty σ_r can be calculated by taking the variance of this expression, which is given by

$$\sigma_r^2 = \hat{\alpha}_r^T\hat{\alpha}_r + 2\text{tr}(\hat{\beta}_r^T\hat{\beta}_r) \tag{6}$$

where tr() is the matrix trace operator.

For simulations of the experimental measurements, the $\mathbf{a}_r$ and $\mathbf{b}_r$ are calculated numerically using the sensitivity-analysis-based method (SAB).[30] For rate constants and rate constant ratios, $\mathbf{a}_r$ can be calculated explicitly. Reaction rate constants are expressed in the Arrhenius form, $k = AT^b \exp(-E/T)$, with some nominal value $k_0 = A_0T^b \exp(-E_0/T)$. The logarithm of the ratio of the rate constant to its nominal value is

$$\ln\frac{k}{k_0} = \ln\frac{A}{A_0} + \frac{E_0 - E}{T} \tag{7}$$

If the reduced variable associated with A is denoted x_A with uncertainty factor f_A and E likewise x_E and f_E and it is assumed that f_E is small, eq 7 can be expressed in terms of the reduced variables by substituting eq 2, which yields

$$\ln\frac{k}{k_0} = x_A \ln f_A - x_E\frac{E_0(f_E - 1)}{T} \tag{8}$$

A rate constant ratio k_1/k_2 can likewise be expressed as

$$\ln\frac{k_1}{k_2} = x_{A,1}\ln f_{A,1} - x_{A,2}\ln f_{A,2} - x_{E,1}\frac{E_0(f_{E,1} - 1)}{T} + x_{E,2}\frac{E_0(f_{E,2} - 1)}{T} + \ln\frac{k_{1,0}}{k_{2,0}} \tag{9}$$

The uncertainty in the rate constant or rate constant ratio can be calculated using eq 6, with $\mathbf{b}_r = 0$. In the case of a single rate constant, the gradient vector is $\mathbf{J}_r^T = [\ln f_A; -E_0T^{-1}(f_E - 1)]$, and for a rate constant ratio it is $\mathbf{J}_r^T = [\ln f_{A,1}; -\ln f_{A,2}; -E_0T^{-1}(f_{E,1} - 1); E_0T^{-1}(f_{E,2} - 1)]$. In the case of the Prior-model uncertainty for a single rate constant, this gives $(2\sigma)^2 = (\ln f_A)^2 + [E_0T^{-1}(f_E - 1)]^2$. The Prior-model uncertainties of the rate coefficients are assumed to be uncorrelated, so there are no cross terms. For the Posterior model, the uncertainty is $\sigma^2 = \mathbf{J}_r^T\sum^*\mathbf{J}_r$. In the Posterior model, rate coefficients are correlated because of nondiagonal terms of the covariance matrix, which in turn comes from information in the experimental measurements.

Experimental Consistency Analysis. It is not always possible to generate a model that simultaneously reproduces all observations. This could be caused by inconsistency between measurements, meaning that the uncertainty on the measurements has been underestimated; it could also be caused by an underestimated uncertainty in the rate coefficients or by a missing chemical pathway. A method of identifying inconsistent observations was proposed in ref 26, iteratively removing these observations from the target set until a self-consistent set is generated. In this procedure, the consistency function $\mathcal{F}_r$ is defined as

$$\mathcal{F}_r = \left| \frac{\eta_r(x^{(0)*}) - \eta_r^{\text{obs}}}{2\sigma_r^{\text{obs}}} \right| \quad (10)$$

If $\mathcal{F}_r > 1$, then the rth experimental target is inconsistent. If there is only one such inconsistent observation, it is removed. If there is more than one, then a strength function S_r is defined as

$$S_r = \mathbf{J}_r \frac{\partial \mathbf{x}^{(0)*}}{\partial \eta_r^{\text{obs}}} \quad (11)$$

which is the normalized scalar product between the Posterior model vector and the model response gradient. This function was chosen because the optimized model vector will tend to move such that it is parallel to the response surface gradient of highly inconsistent targets. Inconsistent observations are ranked by the product $\mathcal{F}_r S_r$, and the one with the largest such value is removed from the data set. The procedure is iterated until all targets are consistent with the Posterior model.

5. RESULTS AND DISCUSSION

5.1. Time Dependence of Product Formation. Model Results. As part of our experimental design process, the behavior of the system was simulated for various mixtures. Figure 2 shows a representative example of the modeled species mole fractions versus time for a mixture reacting at 1000 K and containing 50 μL/L of *t*BPO and 10000 μL/L of *n*-butane. Results are qualitatively similar at other temperatures and for other tBPO mixtures. The postshock quench was simulated as an instantaneous adiabatic cooling to 300 K. Because of the rapid drop in temperature in the postshock expansion and the exponential dependence of rate constants on inverse temperature, the final product amounts are little affected by the exact form of the quenching simulation. Figures 3 and 4 show similar plots for mixtures containing 50 μL/L of HME and 10000 μL/L and 1000 μL/L of *n*-butane, respectively. These data show general features of the two systems and provide information useful in selecting appropriate measurement targets.

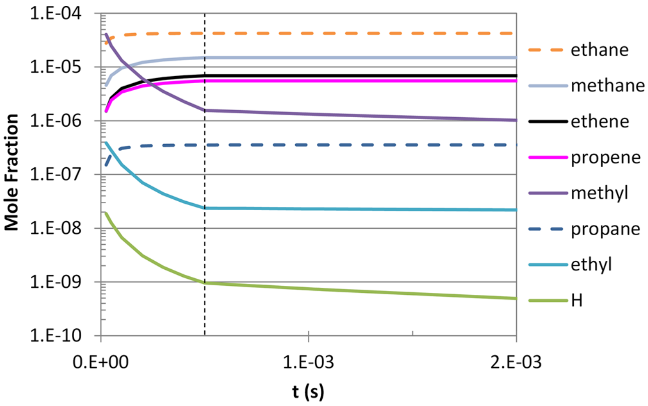

Figure 2. Modeled species mole fractions vs time for mixtures of 50 μL/L of *t*BPO and 10000 μL/L of *n*-butane. Shock conditions: 1000 K, 200 kPa, and τ = 500 μs. The dashed vertical line indicates the start of the quenching period.

For the *t*BPO system, Figure 2 shows that the main stable products methane, ethane, ethene, and propene are essentially completely formed well before the cooling of the shocked gas that occurs at about 500 μs. This is a result of the use of a pulse source of methyl radicals, the rapid recombination rate of CH_3, and the limited ability of the system to propagate radical chains. Radical concentrations follow the order $[CH_3] \gg [C_2H_5] \gg [H]$.

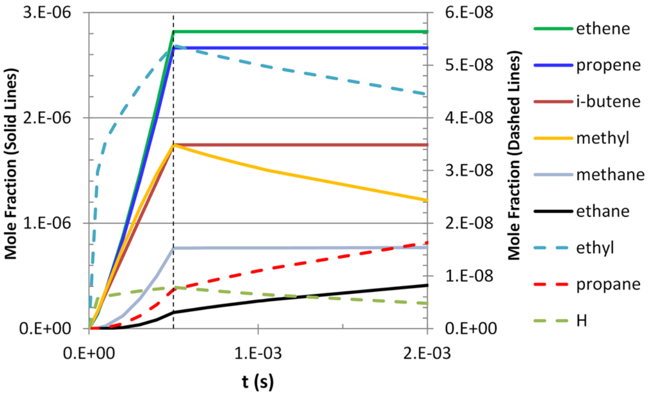

Figure 3. Modeled species mole fractions vs time for mixtures of 50 μL/L of HME and 10000 μL/L of *n*-butane. Shock conditions: 1000 K, 200 kPa, τ = 500 μs. Solid and dashed product lines are referenced to the left and right vertical axes, respectively. The dashed vertical line indicates the start of the quenching period.

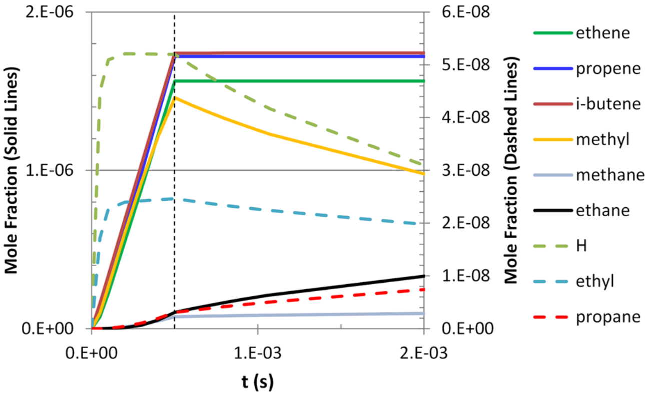

Figure 4. Modeled species mole fractions vs time for mixtures of 50 μL/L of HME and 1000 μL/L of *n*-butane. Shock conditions: 1000 K, 200 kPa, and τ = 500 μs. Solid and dashed lines are referenced to the left and right vertical axes, respectively. The dashed vertical line indicates the start of the quenching period.

On the other hand, with HME as the radical precursor, Figures 3 and 4 indicate that the olefin product concentrations rise rapidly throughout the shock-heated period and then plateau immediately at the start of postshock cooling. This reflects that the main attacking radicals are H atoms and that these are generated throughout the shock-heated period, rather than as an initial pulse. The plateau indicates that H atom concentrations are too low to impact alkene amounts during the quench. Quite different in behavior are the saturated products ethane and propane, which are formed primarily by recombination reactions involving methyl radicals. In contrast to the *t*BPO system, significant fractions of these species are formed in the quench in the HME system. The change in behavior is due to the fact that methyl radicals are secondary products in the HME system and thus have correspondingly low absolute concentrations and low recombination rates. As a result, the concentration of CH_3 builds during the shock heating period in the HME system (rather than decreasing as in the *t*BPO system), and consequently, a significant fraction of the methyl recombination products form during the quench. While the methyl radical concentration is much lower when the

DOI: 10.1021/acs.jpca.5b01004
J. Phys. Chem. A 2015, 119, 7637−7658

precursor is HME rather than *t*BPO, it is still larger than that of H atoms in both systems. This is a consequence of the much higher reactivity of H compared with CH_3.

In our previous experimental design study,[4] we discussed the impact of uncertainty in the reaction time on the predicted product concentrations. The uncertainty in the reaction time is approximately 50 μs. In both HME and *t*BPO systems, the corresponding uncertainty in the ratios of the concentrations of the main products is always less than 1%, and the uncertainty in the absolute product concentrations is less than 5% in the *t*BPO system. These uncertainties are negligible compared to the measurement uncertainty of 10 to 20%. In the HME system, the simulated absolute product concentration has an uncertainty of nearly 15%, which is not negligible. This uncertainty has been considered by folding it into the observed measurement uncertainty.

5.2. Target Measurements and Constraints. Our initial trial optimizations of the Prior model considered only the data from the present experiments with no consideration of target data from the literature. These analyses identified problems with key rate constants and branching ratios for butyl radical decomposition in the Prior model. As discussed below, the Prior model was therefore updated based on recent studies at NIST on related systems before carrying out a subsequent optimization based only on the current data. With this in hand, a more thorough final analysis taking into account data reported in the literature from studies at other temperatures was performed. This analysis includes a review of the literature data and the selection of additional targets from the literature. The respective targets from the current experiments and the literature have been summarized in Tables 2 and 3; these are subsequently discussed in detail.

5.2.1. Target Measurements from Current Experiments. Ethene and Propene. Our MUM-PCE analysis requires the selection of appropriate measurement targets. In the current experiments, ethene and propene product amounts are a key measure of k_s/k_p, the relative rate of radical attack on the secondary and primary hydrogens of *n*-butane. For *t*BPO systems, the relative and absolute amounts of these olefins were targeted, as were the absolute amounts of CH_4 and C_2H_6. Methane and ethane quantities were not targeted for the HME studies because of significant continued formation of these products in the postshock quenching period (see Figures 2−4). Unlike the *t*BPO case, in systems utilizing HME, the olefin product concentrations increase rapidly throughout the shock-heated period, with the consequence that uncertainties in the reaction time impact the results. The ratio of C2/C3 olefin products, however, is only weakly dependent on the reaction time.[4] Both relative and absolute ethene and propene concentrations were included as targets in the HME system, but, as discussed in Section 5.1, a higher uncertainty was assigned to the absolute amounts. Despite this, we note that the modeled absolute product amounts are in excellent agreement with experiment in the HME system. This suggests that errors in the heating times are small.

Butenes. Initial fits with the Prior model showed that butene concentrations were overpredicted by about 1 order of magnitude compared with the experiment. Butene formation channels, predominantly beta C−H scission in butyl radicals (Section 3), compete directly with formation of ethene and propene, and thereby impact derived rate parameters for the title reactions. Examination of the Prior model showed that absolute rate constants for butyl radical decomposition appear to be too small, particularly for the 2-butyl radical. More importantly, the Prior model branching ratio for C−C versus C−H bond scission in the butyl radicals is significantly at odds with the current data, as well as our recent studies of the related decomposition of pentyl radicals.[15−17] The discrepancy in the branching ratio is about 1 order of magnitude and fell outside of the uncertainties initially estimated in the JetSurf 2 model. The source of the parameters in JetSurf is not clear, but prior to optimization, we have updated the rate constants for decomposition of 1-butyl and 2-butyl radicals. Our revised values are based on NIST results on the decomposition of pentyl radicals,[15−17] which should have high pressure rate constants that are very similar to butyl radicals for analogous reactions. The NIST model of pentyl radical decomposition[15−17] is derived from an RRKM master equation analysis that is based on computed molecular structures and reaction energetics that were then minimally tuned to reproduce a variety of experimental data, including pressure-dependent branching ratios and high and low temperature kinetic results for bond scissions and the reverse addition reactions. As a whole, it appears to be the most complete kinetic analysis of the pentyl system currently available. As discussed in our earlier work,[17] our fitted rate constants for beta C−C scission in the pentyl system use as key data the results of Knyazev and co-workers on the decomposition of 1-butyl[31] and 2-butyl,[32] and are thus compatible with those works. We do not directly use rate parameters from those works, however, because their model does not include the C−H bond scission channels, and the main issue in the present case is a reasonable starting value for the branching between C−C and C−H scission. Specific changes to the JetSurf 2 based Prior model included setting the high pressure limit for beta C−C scission in 1-butyl equal to that of 1-pentyl. For 2-butyl, the high pressure limit for beta scission of methyl was set equal to that for methyl scission in 3-pentyl. Analogous approximations were made for the C−H scission channels, which are relatively minor pathways. The k_∞/k_0 ratios for butyl radicals were not altered from those currently used in JetSurf 2. A more complete analysis of the butyl system would be desirable, but the above should provide reasonable kinetics and, in particular, more accurate branching ratios for C−C and C−H bond scissions in the Prior model, which is what is needed for present purposes. Butene concentrations and butene/ethene and butene/propene ratios from selected experiments were then added as targets as given in Table 2.

Propane and Ethane. At the lower temperatures of our study, the ejection of H from ethyl radical, R252, becomes slow enough that recombination with methyl, R279, becomes competitive in the *t*BPO experiments, where methyl radical concentrations are large. Experimentally, the observed ratios of propane to ethene indicate that recombination accounts for about 25% of ethyl radicals at 850 K, dropping to about 10% at 1000 K. Ethyl radicals lost as propane impact the ethene to propene ratio and, thus, the interpretation of these data in terms of the k_s/k_p relative rate. Propane quantities were therefore targeted in the analysis of the *t*BPO system data. In the HME system, the recombination reaction is negligible because of a combination of lower methyl radical concentrations, and generally higher temperatures, which rapidly reduce the unimolecular lifetime of ethyl radicals.

Ethane formation, dominated by recombination of methyl radicals, was targeted in *t*BPO experiments where initial methyl radical concentrations are large and formation of ethane is largely complete at the end of the shock heating period. In experiments with HME, where concentrations of CH_3 are much lower, the model indicates (Figure 3) that a significant fraction of the ethane is formed in the quench; ethane concentrations were not targeted for those experiments.

5.2.2. Parameter Sensitivities. The sensitivities of the target measurements to the kinetic parameters in the Prior model (after updating the butyl radical kinetics as described above) have been investigated. Logarithmic sensitivity coefficients were calculated using the formula $\mathcal{S}_{r,i} = (d\eta_r/d\theta_i)(\theta_i/\eta_r)$, where η_r is the simulation-predicted value of measurement r, θ_i is a generalized rate parameter.

Ethene and propene products are the targets most closely related to the title reactions, and representative sensitivity-coefficient plots are presented for mixtures D (HME) and G (*t*BPO) in Figure 5. Results for related mixtures are similar, and additional plots are given in the Supporting Information. It is immediately apparent from Figure 5 that the C_2H_4/C_3H_6 ratios are highly sensitive to the k_s and k_p values of the title reactions, and that the respective experiments with HME and *t*BPO precursors successfully separate the behavior of H atoms and methyl radicals. With regard to the temperature dependence of the sensitivities, the analyses show that experiments at lower temperatures, where the chemistry is less complex, are better at isolating the title reactions. This is particularly true for the *t*BPO system, wherein the results become increasingly less sensitive to $k_p(CH_3)$ at temperatures above 1050 K. At these higher temperatures, abstractions by H atoms and the unimolecular decomposition of *n*-butane are increasingly important.

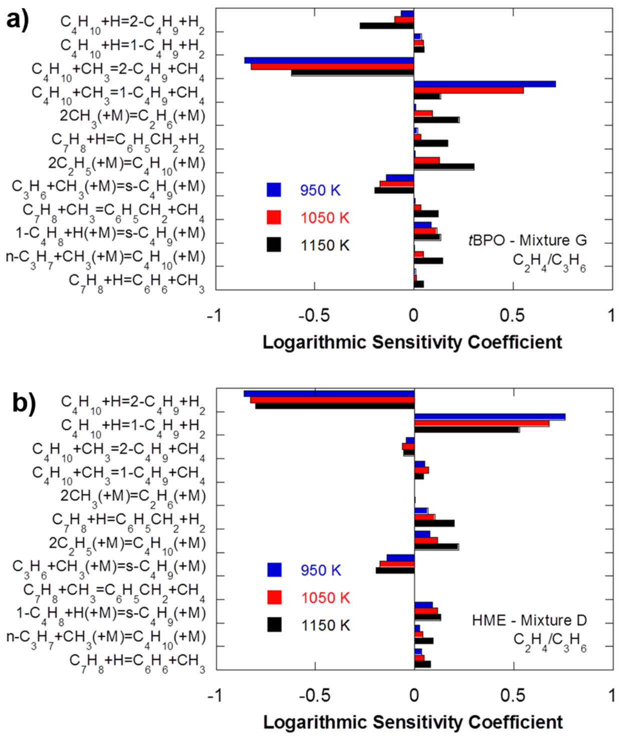

Figure 5. Sensitivity of the measured C_2H_4/C_3H_6 ratios to selected reactions over a range of temperatures.

Additional sensitivity plots, including those pertinent to various minor species targets, are given in the Supporting Information. The general features are as one would anticipate. For instance, in the *t*BPO system (methyl radicals), ethane and methane are sensitive to methyl recombination in competition with the H abstraction reactions of methyl. In both *t*BPO and HME systems, butene products are highly sensitive to the beta scission reactions of the intermediate butyl radicals, as well as the abstraction reactions that form the butyl radicals. Benzene is sensitive to displacement of methyl from the toluene inhibitor by H atoms in competition with the H abstraction reactions of H. In general the rate constants related to formation of butenes and benzene are more cleanly defined by the studies with HME.

Overall, the sensitivity analyses show that multiple reactions have some impact on the kinetics of interest, thus justifying the use of modeling in analyzing the results, but that the title reactions are nonetheless the dominant determinants of the ethene and propene targets. The rate constants we seek to measure should therefore be accurately defined at temperatures near 1000 K by the present experiments. Table 4 presents rate constants derived for the title reactions when considering only the present experimental data. The only constraints of Table 3 that were included in this analysis are those pertaining to dissociation of the 2-butyl radical and those related to the geometric mean rule for radical recombination reactions.

To better describe the rate parameters over a wide range of temperatures, we have carried out an additional analysis which includes various data from the literature. These data are reviewed in the following section of this report.

5.2.3. Target Measurements from the Literature: A Review. H Abstraction by Methyl Radicals. Relative Values of $k_s(CH_3)$ and $k_p(CH_3)$. For methyl radicals, literature results pertaining to lower temperatures (roughly 400 to 700 K) have been reviewed by Kerr and Parsonage[33] in 1976. They recommend generic rate constant values for abstraction of primary and secondary H by methyl, $k_p(CH_3)$, and $k_s(CH_3)$, based on an evaluation of data on the C2 to C4 alkanes from a number of researchers, and making the usual assumption from experiment[34,35] and

Table 4. Posterior Rate Coefficients Derived without Inclusion of the Literature Measurements of Table 3[a]

		A^b			E^b			Posterior rate coefficients		
n	title reactions	f_i^b	f_i^{*c}	$\ln f_i^*/\ln f_i$	f_i^b	f_i^{*c}	$\ln f_i^*/\ln f_i$	log 10 A^{*c}	b^{*c}	E^*/R (K)^c
633	$C_4H_{10} + H \leftrightarrow pC_4H_9 + H_2$	3	1.61	0.43	1.2	1.11	0.56	6.06 ± 0.21	2.54	3246 ± 349
634	$C_4H_{10} + H \leftrightarrow sC_4H_9 + H_2$	3	1.63	0.45	1.2	1.16	0.82	6.44 ± 0.21	2.4	2340 ± 377
	$(k_p)/(k_s)$							−0.38 ± 0.18	0.14	906 ± 460
643	$C_4H_{10} + CH_3 \leftrightarrow pC_4H_9 + CH_4$	3	1.42	0.32	1.2	1.1	0.55	0.142 ± 0.15	3.65	3036 ± 318
644	$C_4H_{10} + CH_3 \leftrightarrow sC_4H_9 + CH_4$	3	1.44	0.33	1.2	1.13	0.66	0.86 ± 0.16	3.46	2585 ± 332
	$(k_p)/(k_s)$							−0.718 ± 0.18	0.19	451 ± 488

[a] All uncertainties are 2σ. [b] $k = AT^b \exp(ER^{-1}T^{-1})$. Logarithmic uncertainty $\sigma = 1/2 \log f$. [c] Starred quantities refer to the Posterior model, while unstarred quantities refer to the Prior model.

thermochemical kinetics[36] that rate differences for analogous C−H bonds are small. Most of the available data refer to absolute measurements of overall rates, with relative rates derived on the basis of additional assumptions. The Kerr and Parsonage evaluations have been accepted and used by most subsequent reviewers, including Tsang in his seminal compilation and evaluation of reactions important in propane combustion,[1] a work to which most existing hydrocarbon combustion models are traceable.

We have re-examined the existing data and note certain problems. At lower temperatures, two measurements of the relative rate for methyl attack on butane were available to Kerr and Parsonage, and these remain the most direct measurements in this regime. McNesby and Gordon[37] in 1956 photolyzed acetone-d_6 to generate CD_3 in the presence of *n*-butane or *n*-butane-2,2,3,3-d_4 at temperatures between 522 and 723 K. Competitive attack of CD_3 on butane and acetone-d_6 occurs, and relative rate constants were determined from the observed amounts of CHD_3 and CD_4. McNesby and co-workers later used the same technique to study propane and propane-2,2-d_2.[34,35] Kerr and Parsonage derived absolute rate constants from these studies using the CD_3 + acetone-d_6 reaction as a reference. In 1966, Tedder and Watson[38] photolyzed azomethane to generate CH_3 in the presence of *n*-butane, trapped the intermediate butyl radicals by iodination with methyl iodide, and derived relative rates on the basis of the distribution of isomeric butyl iodides. Their data span the temperature range from 371 to 492 K. They report $k_s(CH_3)/k_p(CH_3) = (1.21 \pm 0.16)\exp[(831 \pm 50\ K)/T)]$, where $k_s(CH_3)/k_p(CH_3)$ is the ratio of abstraction of H from the secondary and primary sites *on a per hydrogen basis*. However, in their later analysis, Kerr and Parsonage appear to take these values (text on p 45 and Figure 8 of Kerr and Parsonage[33]) to be on an absolute and not per H basis. This creates a discrepancy at low temperatures of about a factor of 1.5 with the generic values of $k_s(CH_3)$ and $k_p(CH_3)$ recommended by Kerr and Parsonage.

Data not considered by other reviewers include the 1968 results of Leathard and Purnell,[39] who used a static system to investigate the pyrolysis of propane at small extents of reaction between 783 and 833 K. They derived k_s/k_p values on the basis of product ratios and a complex kinetic analysis, which included the assumption that k_s/k_p values for H and CH_3 are identical. This result is less direct than the other measurements but is in very good agreement with the results of the present experiments. The most recent data of which we are aware are those of Sway,[40] who in 1990 reported absolute rate constants between 399 and 434 K for the reaction of methyl with a series of alkanes, including *n*-butane, neopentane, cyclohexane, and HME. Using a static reactor, methyl was generated at total pressures of about 70 kPa in a nitrogen bath gas from the thermal decomposition of a small amount of *t*BPO in the presence of the alkane. Methane and ethane were monitored by GC analysis, and abstraction rate constants determined relative to recombination of methyl radicals. These data lead to $k_s(CH_3)/k_p(CH_3)$ values for *n*-butane if one assumes that the per H $k_p(CH_3)$ rate constants in *n*-butane are the same as those determined by Sway for neopentane or HME. There is, however, about a factor of 2 variation in the derived $k_s(CH_3)/k_p(CH_3)$ values depending on which reference compound is used for $k_p(CH_3)$. Alternatively, using the Sway data for cyclohexane to establish $k_s(CH_3)$ gives nearly the same result. The derived values bracket the results of Tedder and Watson but require added assumptions.

While we would like to see more modern methods applied to the determination of $k_s(CH_3)/k_p(CH_3)$ values at lower temperatures, the four studies discussed above use different methodologies at different temperatures and arrive at results that are self-consistent with each other and with the present work, which suggests that there are no major errors. In our final analyses, we have selected as targets the most direct measurements specific to *n*-butane, taking the $k_s(CH_3)/k_p(CH_3)$ values determined by McNesby and Gordon[37] and the result of Tedder and Watson[38] as reported in their original paper.

H Abstraction by Methyl Radicals. Absolute Rate Constants. Absolute values of $k_s(CH_3)$ and $k_p(CH_3)$ for *n*-butane at lower temperatures can be estimated by coupling the overall rate constant measured by Sway with the preferred $k_s(CH_3)/k_p(CH_3)$ values. Alternatively, the results of Sway for neopentane and HME directly yield $k_p(CH_3)$ for these compounds, and these data can be scaled to *n*-butane based on the number of primary hydrogens. Both methods give similar results. One can also derive an independent estimate of $k_s(CH_3)$ from the Sway data on cyclohexane, which has only secondary hydrogens (albeit cyclic). This method requires no assumption of the $k_s(CH_3)/k_p(CH_3)$ value. It also leads to a very similar result, indicating consistency of the various data. In the end, we have assumed that per H $k_p(CH_3)$ values for *n*-butane are the average of those for HME and neopentane, with an uncertainty of a factor of 2, and have targeted the Sway measurements on this basis.

Sway's measurements were obtained relative to the well-established rate constant for recombination of methyl radicals under pressure conditions (70 kPa) where the reaction is close to the high pressure limit. Given that the rate of methyl recombination is only weakly dependent on temperature, and that the present results are linked to the same reaction, this should minimize systematic discrepancies in the high and low temperature results and lead to a self-consistent estimate of the $k_s(CH_3)$ and $k_p(CH_3)$ temperature dependencies. The methyl recombination rate used by Sway is very close to that used in the Prior model (and is little changed in our final fit), with normalization requiring adjustments of the derived $k_s(CH_3)$ and $k_p(CH_3)$ values of <2.5%.

Also relevant are experiments relating to the kinetics of CH_3 + C_2H_6 at high temperatures. While not specific to butane, these can be used to limit the possible value of $k_p(CH_3)$, particularly at temperatures higher than studied here. Peukert et al.[41] in 2013 reported a shock tube investigation of CH_3 + C_2H_6 at temperatures of 1153 to 1297 K, generating methyl from a thermal precursor, using ARAS (atomic resonance absorption spectroscopy) to monitor H atoms formed in the decomposition of the initial ethyl radical product and then modeling the time-dependent decays to derive the kinetics. In earlier work, Roth and Just[42] also used H atom ARAS and modeling to derive rate constants for CH_3 + C_2H_6 at 1460 to 1600 K from shock tube experiments of ethane pyrolysis. To constrain rate constants for CH_3 + *n*-butane, we have included as targets the rate constants of Peukert et al. for CH_3 + ethane, while requiring $k_p(CH_3 + \text{ethane}) = k_p(CH_3 + n\text{-butane})$ within a factor of 2.

H Abstraction by Hydrogen Atoms. Relative Values of k_s(H) and k_p(H) from the Literature. A number of studies and evaluations are available for abstraction of H from *n*-butane and related hydrocarbons. The data, though sparse, are in general accord with the expectation from thermochemical kinetics that per H k_s and k_p rate constants are approximately equal for all *n*-alkanes and that one may scale values for different hydrocarbons based on the number of hydrogens of a given type.

In 1979, Baldwin and Walker[43] reported rate constants at 753 K for the reaction of H with alkanes from studies of slowly reacting mixtures of H_2 and O_2 in the presence of various C2 to C5 hydrocarbons, including *n*-butane. Absolute rate constants were derived relative to H + O_2, and generic values of $k_s(H)/k_p(H)$ were derived by comparing molecules with differing numbers of primary and secondary hydrogens. These results supersede the previous analysis by Baker, Baldwin, and Walker.[44]

Tsang's 1988 recommendation for propane[1] is based on measurements of the overall rate constant by Lede and Villermaux[45,46] and Marshall et al.,[47] together with consideration of the rate data on H + ethane, the $k_s(H)/k_p(H)$ value of Baldwin and Walker,[43] and a fit to the preferred data using a BEBO transition state. In 1991, Cohen[2] reviewed the literature on H plus alkane reactions, derived $k_s(H)/k_p(H)$ values by comparing absolute rate constants for a series of molecules, and used the transition state theory to model and extrapolate the results. Cohen's $k_s(H)/k_p(H)$ values are roughly a factor of 1.5 to 2 larger than Tsang's. The source of the rate parameters used in JetSurf 2 (the Prior model) for butane is not clear, but the derived per H $k_s(H)/k_p(H)$ values are roughly 30% larger than those of Tsang for propane over the full temperature range.

The most direct low-temperature measurements of $k_s(H)/k_p(H)$ are those of Campbell et al.,[48] who in 1969 reported values for the reaction of H with propane between 318 and 413 K. They created H atoms from the mercury-sensitized photodissociation of H_2 and derived relative abstraction rates based on the observed radical recombination products of the isomeric propyl radicals. The primary product data were corrected for disproportionation reactions based on the data of Terry and Futrell.[49] This correction has some impact on $k_s(H)/k_p(H)$, but the disproportionation values have been consistently confirmed in later work[50−52] and reviews.[1,53] Neither Tsang[1] nor Cohen[2] appear to use the Campbell et al.[48] data in their reviews. Tsang's recommended $k_s(H)/k_p(H)$ values are nonetheless only 15% to 25% lower than these results, while Cohen's values are roughly a factor of 2 larger. Differing substantially from the Campbell et al. report are the less-directly obtained values of Nicolas and Vaghjiani,[54] who in 1989 photochemically created H atoms at specific energies and monitored the integrated reaction probabilities for reaction with the primary and secondary sites of *n*-butane. They used these data to derive reaction cross sections, threshold energies, and ultimately $k_p(H)$ and $k_s(H)$ values for the thermal reactions at temperatures from 250 to 500 K. They do not provide details of their derivation of the thermal rate constants, but $k_s(H)/k_p(H)$ values from their rate expressions are roughly 5 to 20 times larger than the other literature data. These results were not used. The intermediate temperature result of Baldwin and Walker[43] relies on a complex model and was likewise not specifically targeted, although our final fit is in excellent agreement. As a low-temperature target for $k_s(H)/k_p(H)$, we have included only the data of Campbell et al.,[48] which represent the most direct measurement, assigning a 2σ uncertainty of about 40% (Table 3).

H Abstraction by Hydrogen Atoms. Absolute Rate Constants from the Literature. Although there are no direct determinations of $k_p(H)$ or $k_s(H)$ for *n*-butane at low temperatures, values may be derived through the relative rate measurements, and there are direct measurements for some related *n*-alkanes. The extant data show a reasonable degree of consistency. The relative rate of reaction of H atoms with *n*-butane and the olefin propene at 297 K has been determined by Jennings and Cvetanovic.[55] Yang,[56,57] at temperatures of 300 to 500 K, also investigated rates relative to reaction of H with propene for a series of alkanes, including ethane, propane, *n*-butane, and isobutane. In the experiments with propane, Yang further employed the H + ethene reaction as an additional standard.

The absolute rate constant for the H + propene reference reaction used in the above studies has been directly determined by several researchers[58−63] on the basis of H atom decay rates, and the results are in very good agreement. These data, in conjunction with $k_s(H)/k_p(H)$, lead to absolute values of $k_s(H)$ and $k_p(H)$ for *n*-butane. The data of Yang allow the similar extraction of $k_p(H)$ values for ethane and propane. For all three alkanes, the derived $k_p(H)$ values are equal within about 25% at 300 K, which suggests that it is reasonable to consider absolute measurements of $k_p(H)$ for ethane and propane in our assessment. The largest body of data pertain to ethane. The most recent direct study is that of Bryukov et al.,[64] who used a flow reactor and a discharge flow/resonance fluorescence technique to monitor H atom decays in the presence of excess ethane. They also present a thorough review of the Prior direct measurements in their 2001 report. In the midtemperature region, the combined direct measurements of Jones et al.[65] and Bryukov et al.[64] span 400 to 800 K and are in good agreement. Direct measurements at lower temperatures by other researchers[45,66,67] require stoichiometric corrections of up to a factor of 4 based on the assumed reaction mechanism. Bryukov et al. argue that inconsistent application and ambiguity in these corrections leads to uncertainty in the rate constant at ambient temperatures, and that these other measurements fall outside of a transition-state theory extrapolation of the higher temperature data. Nonetheless, the rate constants from the direct low-temperature studies questioned by Bryukov et al. are in accord with those derived from the relative rate measurements[55−57] discussed above when using absolute values of the alkene reactions H + propene or H + ethene as the reference. With respect to the temperature extrapolation, if one accepts the ambient temperature measurements, the empirical temperature dependence of $k_p(H)$ that is required to fit the data is similar to that derived by Kerkeni and Clary[68,69] using quantum chemistry calculations and reduced dimensionality quantum dynamics. We have elected to retain the results at ambient temperatures in deriving our fit. However, to prevent undue weighting of particular methodologies with their attendant systematic uncertainties, we have included only one representative example of each type of experiment. Specific targets are given in Table 2. To constrain rate constants for H + *n*-butane, while taking into account the related measurements for H + ethane, we have targeted measured values of H + ethane, while requiring k_p(H + ethane) = k_p(H + *n*-butane) within a factor of 2.

Additional Constraints. Additional constraints added to the model were a requirement that rate constants for interrelated radical recombination reactions follow the well-documented geometric mean rule[70] within 20%, and, for pressure-dependent rate constants, that the relative values of k_0 and k_∞ remain fixed at those in the Prior model. These constraints ensure that physically realistic values for these rate constants are maintained during the optimization.

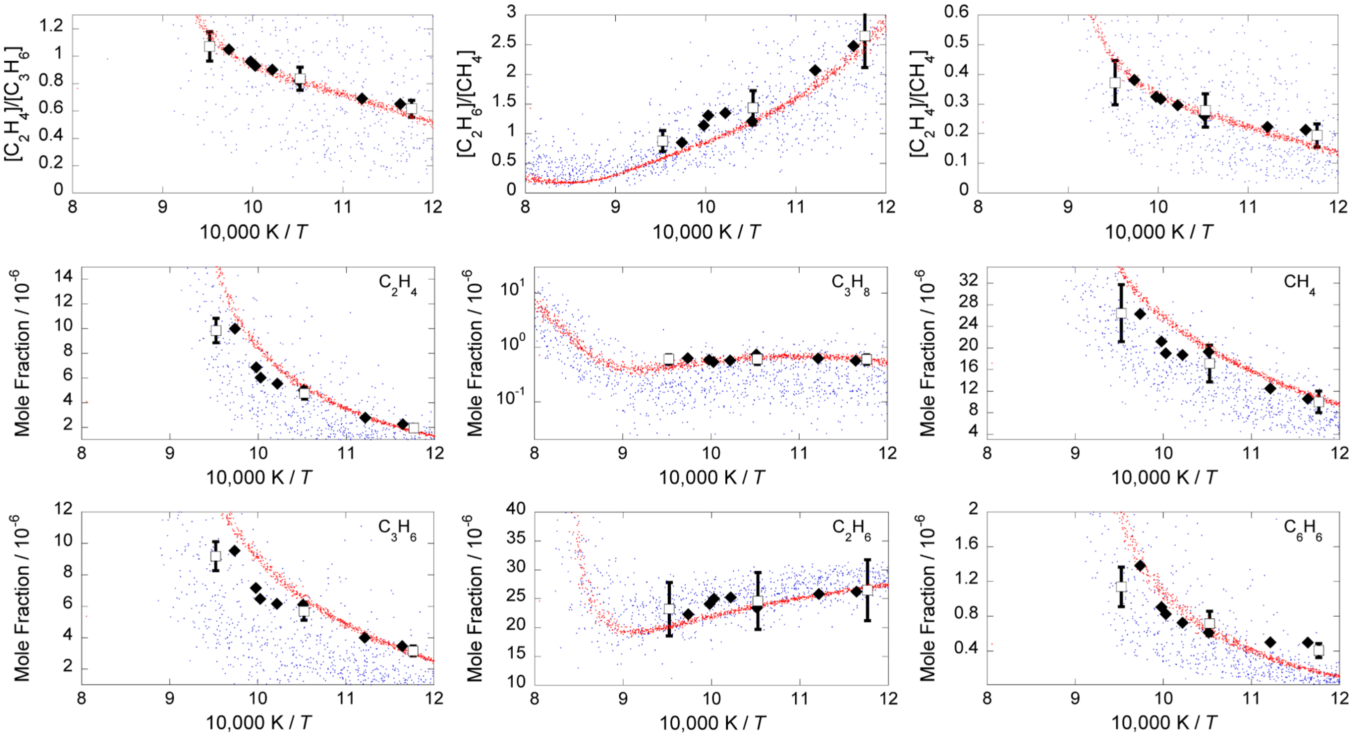

Figure 6. Comparison of selected experimental and modeled results for mixture A, *t*BPO precursor. Blue points are a Monte Carlo sampling of the Prior model uncertainty. Red points are a Monte Carlo sampling of the Posterior model uncertainty. ◆'s indicate experimental measurements, and □'s indicate the specific target values of Table 2.

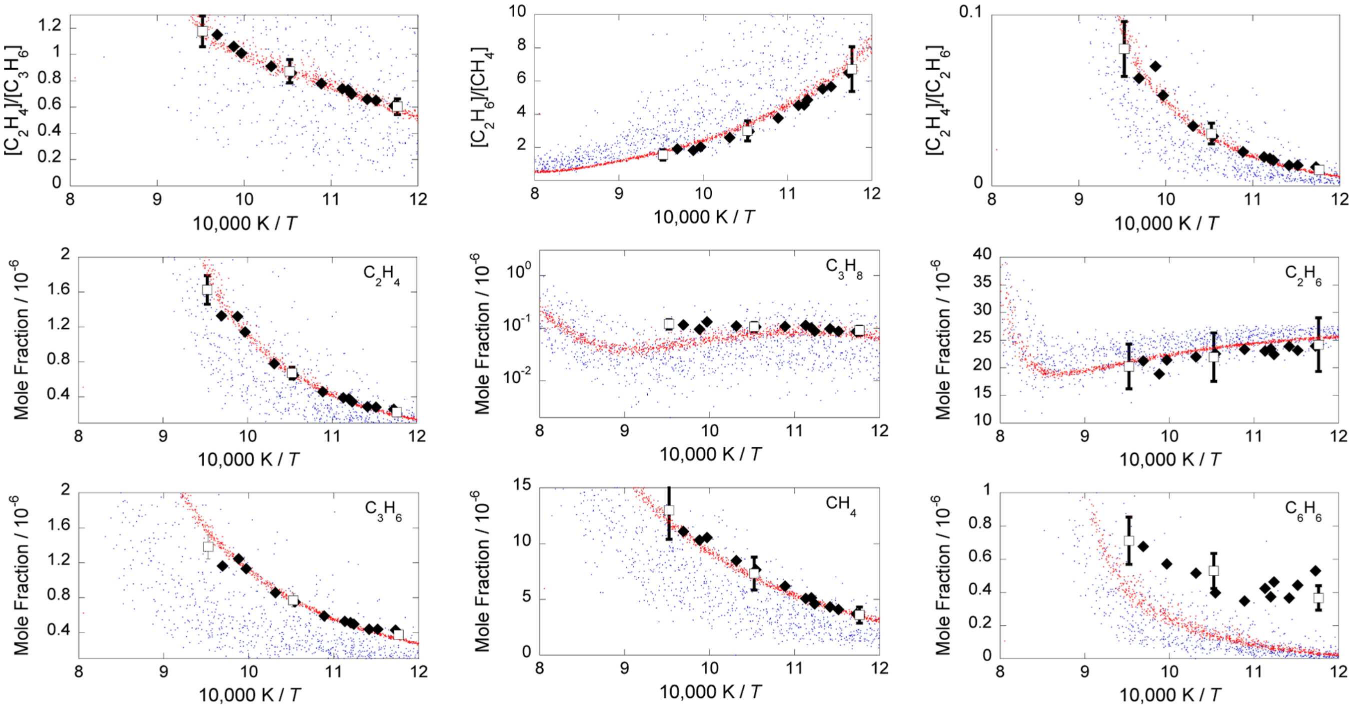

Figure 7. Comparison of selected experimental and modeled results for mixture F, *t*BPO precursor. Blue points are a Monte Carlo sampling of the Prior model uncertainty. Red points are a Monte Carlo sampling of the Posterior model uncertainty. ◆'s indicate experimental measurements, and □'s indicate the specific target values of Table 2.

5.3. Modeled Species Profiles. Selected experimental results are compared with the Prior and Posterior models in Figures 6, 7, and 8. In these plots, the blue points pertain to the Prior model and the red to the Posterior model. All experimental data points are shown in the figures, with the targeted values of Table 2 indicated as unfilled squares. The significantly reduced scatter in the Posterior model results is indicative of marked improvement in the relevant rate parameters after conditioning with the present experiments.

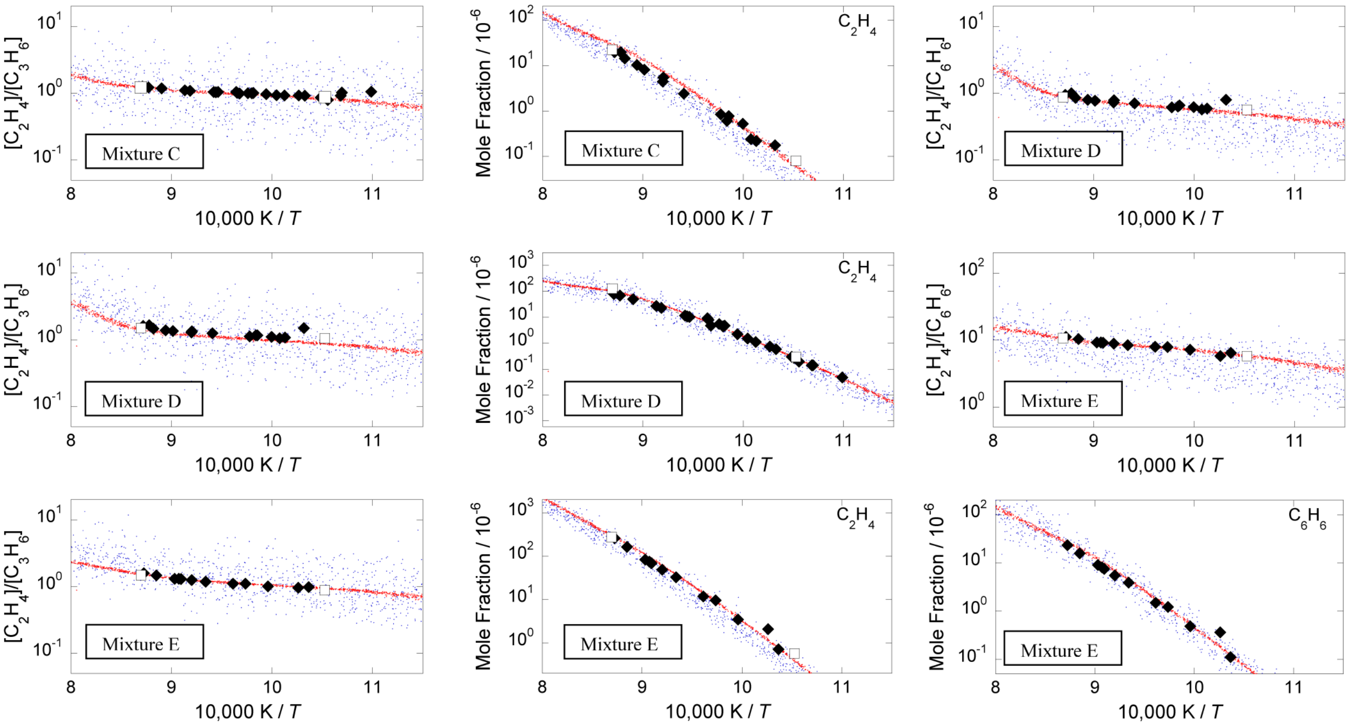

Figure 8. Comparison of selected experimental and modeled results for mixtures C, D, and E and the HME precursor. Blue points are a Monte Carlo sampling of the Prior model uncertainty. Red points are a Monte Carlo sampling of the Posterior model uncertainty. ◆'s indicate experimental measurements, and ☐'s indicate the specific target values of Table 2.

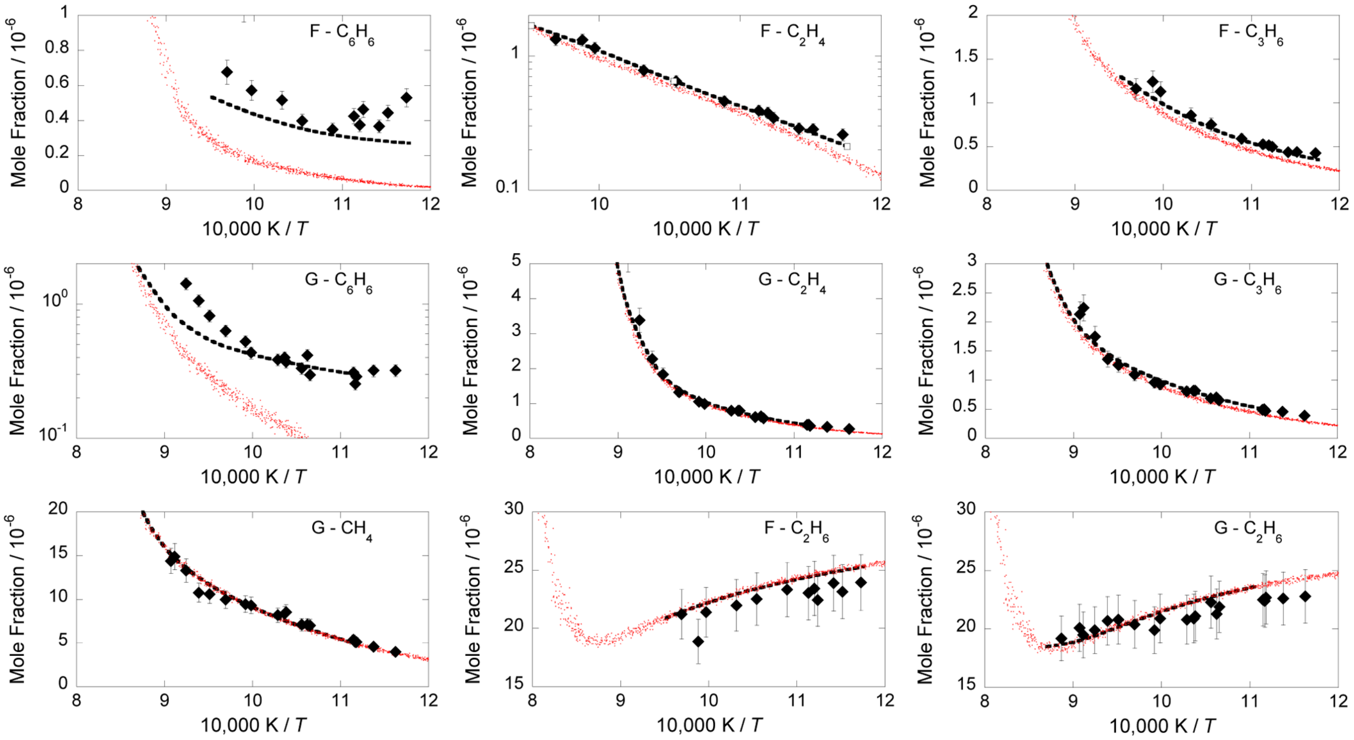

Figure 9. Posterior model with small added artificial source of H atoms. Red points indicate the original Posterior model, dashed lines the same model augmented with a 1 ppm source of H atoms.

Model results are in generally good agreement with experiment for all mixtures and olefin ratios are well-predicted in all systems. Absolute product amounts are also in excellent agreement with the experiment for both the *t*BPO and HME systems. In some of these plots, there is subtle curvature in the data, which could be interpreted as experimental scatter, but is actually reproduced quite well by the model. This suggests that the model provides a more accurate and realistic description of the systems than would be achieved with analyses based on simplified chemistry.

Table 5. Rate Coefficient Uncertainties and Posterior Values Derived Utilizing the Constraints of Tables 2 and 3[a]

		A[b]			E[b]			Posterior rate coefficients				
n	name	f_i[b]	f_i^*[c]	$\ln f_i^*/\ln f_i$	f_i[b]	f_i^*[c]	$\ln f_i^*/\ln f_i$	log 10 A^*[c]	b^*[c]	E^*/R (K)[c]		
	Title Reactions											
633	$C_4H_{10} + H \leftrightarrow pC_4H_9 + H_2$	3	1.46	0.34	1.2	1.04	0.23	5.98 ± 0.16	2.54	3511	±	152
634	$C_4H_{10} + H \leftrightarrow sC_4H_9 + H_2$	3	1.46	0.34	1.2	1.08	0.43	6.23 ± 0.16	2.4	2265	±	183
	$(k_p)/(k_s)$							−0.245 ± 0.066	0.14	1246	±	141
643	$C_4H_{10} + CH_3 \leftrightarrow pC_4H_9 + CH_4$	3	1.34	0.27	1.2	1.04	0.23	0.228 ± 0.13	3.65	3650	±	156
644	$C_4H_{10} + CH_3 \leftrightarrow sC_4H_9 + CH_4$	3	1.36	0.28	1.2	1.07	0.35	0.87 ± 0.13	3.46	3024	±	198
	$(k_p)/(k_s)$							−0.641 ± 0.062	0.19	626	±	117
	C−C Bond Fission Reactions											
631	$nC_3H_7 + CH_3(+M) \leftrightarrow C_4H_{10}(+M)$ (k_∞)	2	1.49	0.58	–	–	–	14.45 ± 0.17	−0.32	0		–
	(k_0)							61.59 ± 0.17	−13.24	3030		–
632	$2C_2H_5(+M) \leftrightarrow C_4H_{10}(+M)$ (k_∞)	2	1.27	0.35	–	–	–	14.22 ± 0.10	−0.5	0		–
	(k_0)							61.36 ± 0.10	−13.42	3030		–
	Reactions of Toluene											
673	$C_6H_5CH_3 + H \leftrightarrow C_6H_5CH_2 + H_2$	2	1.75	0.81	1.16	1.10	0.65	13.92 ± 0.24	0	4770	±	485
674	$C_6H_5CH_3 + H \leftrightarrow C_6H_6 + CH_3$	2	1.46	0.55	1.2	1.15	0.78	6.10 ± 0.16	2.17	2093	±	320
676	$C_6H_5CH_3 + CH_3 \leftrightarrow C_6H_5CH_2 + CH_4$	2	1.60	0.68	1.14	1.07	0.51	11.61 ± 0.20	0	4687	±	327
680	$C_6H_5CH_2 + H(+ M) \leftrightarrow C_6H_5CH_3\ (+M)$ (k_∞)	2	1.99	0.99	–	–	–	14.00 ± 0.30	0	0		–
	(k_0)							103.04 ± 0.30	−24.63	7368		–
805	$C_6H_5CH_2 + CH_3 \leftrightarrow C_6H_5C_2H_5$	2	1.30	0.38	1.2	1.20	0.99	18.86 ± 0.11	−1.812	987	±	196
820	$2C_6H_5CH_2 \leftrightarrow (C_6H_5CH_2)_2$	2	1.31	0.39	–	–	–	20.83 ± 0.12	−2.669	672		–
	Reactions of Methyl and Ethyl											
91	$CH_3 + H(+M) \leftrightarrow CH_4(+M)$ (k_∞)	2	1.99	0.99	–	–	–	16.06 ± 0.30	−0.63	193		–
	(k_0)							33.35 ± 0.30	−4.76	1232		–
107	$2CH_3(+M) \leftrightarrow C_2H_6(+M)$ (k_∞)	2	1.22	0.29	–	–	–	16.26 ± 0.09	−0.97	312		–
	(k_0)							50.18 ± 0.09	−9.67	3141		–
108	$2CH_3 \leftrightarrow H + C_2H_5$	5	2.56	0.58	1.2	1.17	0.85	12.40 ± 0.41	0.1	5528	±	929
252	$C_2H_4 + H(+M) \leftrightarrow C_2H_5(+M)$ (k_∞)	3	1.93	0.60	–	–	–	9.33 ± 0.29	1.463	683		–
	(k_0)							39.50 ± 0.29	−6.64	2913		–
264	$C_2H_6 + CH_3 \leftrightarrow C_2H_5 + CH_4$	5	4.92	0.99	–	–	–	5.39 ± 0.69	2	4635		–
279	$C_2H_5 + CH_3(+M) \leftrightarrow C_3H_8(+M)$ (k_∞)	3	2.41	0.80	–	–	–	14.97 ± 0.38	−0.5	0		–
	(k_0)							62.20 ± 0,38	−13.42	3030		–
282	$C_2H_6 + H \leftrightarrow C_2H_5 + H_2$	2	1.42	0.51	1.18	1.04	0.22	8.15 ± 0.15	1.9	3825	±	143
286	$C_2H_6 + CH_3 \leftrightarrow C_2H_5 + CH_4$	2	1.31	0.39	1.13	1.04	0.34	6.90 ± 0.12	1.74	5316	±	223
	Other Secondary Chemistry											
362	$C_3H_6 + H \leftrightarrow C_2H_4 + CH_3$	2	1.97	0.98	1.12	1.12	0.99	21.87 ± 0.29	−2.39	5690	±	673
363	$C_3H_6 + H \leftrightarrow aC_3H_5 + H_2$	2	1.99	0.99	1.2	–	–	5.20 ± 0.30	2.5	1254		–
553	$1\text{-}C_4H_8 + H(+M) \leftrightarrow pC_4H_9(+M)$ (k_∞)	3	2.88	0.96	–	–	–	8.92 ± 0.46	1.323	528		–
	(k_0)							34.59 ± 0.46	−5.34	2418		–
554	$1\text{-}C_4H_8 + H(+M) \leftrightarrow sC_4H_9(+M)$ (k_∞)	3	1.67	0.47	–	–	–	8.49 ± 0.22	1.389	−341		–
	(k_0)							38.31 ± 0.22	−6.11	1255		–
565	$2\text{-}C_4H_8 + H(+M) \leftrightarrow sC_4H_9(+M)$ (k_∞)	3	1.69	0.48	–	–	–	8.29 ± 0.23	1.494	329		–
	(k_0)							38.11 ± 0.23	−6.01	1927		–
573	$iC_4H_8 + H \leftrightarrow iC_4H_7 + H_2$	3	2.97	0.99	1.2	1.20	1.00	6.04 ± 0.47	2.54	3424	±	683
574	$iC_4H_8 + H \leftrightarrow C_3H_6 + CH_3$	3	2.87	0.96	1.2	1.19	0.97	21.91 ± 0.46	−2.39	5551	±	1079
582	$C_2H_4 + C_2H_5 \leftrightarrow pC_4H_9$	3	2.82	0.94	1.2	1.20	0.99	2.59 ± 0.45	2.841	2453	±	484
592	$C_3H_6 + CH_3(+M) \leftrightarrow sC_4H_9(+M)$ (k_∞)	2	1.67	0.74	–	–	–	4.35 ± 0.22	2.393	3730		–
	(k_0)							21.48 ± 0.22	−1.88	−174		–
604	$sC_4H_9 + CH_3 \leftrightarrow C_2H_4 + 1\text{-}C_4H_8$	5	4.95	0.99	–	–	–	14.39 ± 0.69	−0.68	0		–
869	$pC_4H_9 + CH_3 \leftrightarrow nC_5H_{12}$	2	1.99	0.99	–	–	–	14.24 ± 0.30	−0.32	0		–
870	$sC_4H_9 + CH_3 \leftrightarrow iC_5H_{12}$	2	1.99	1.00	–	–	–	15.16 ± 0.30	−0.68	0		–

[a] All uncertainties are 2σ. [b] $k = AT^b \exp(ER^{-1}T^{-1})$. Logarithmic uncertainty $\sigma = 1/2 \log f$. [c] Starred quantities refer to the Posterior model, while unstarred quantities refer to the Prior model. Parameters without listed uncertainties were inactive.

Some discrepancies with the experiment begin to appear at temperatures above 1050 K, where the model increasingly underpredicts the absolute concentrations of the C1 to C3 species. Examination of the model shows that unimolecular decomposition of *n*-butane begins to affect the results at higher temperatures and is more significant for larger *n*-butane/precursor ratios (e.g., mixtures A, B, and E) and larger absolute concentrations of *n*-butane. At these higher temperatures where small but measureable *n*-butane decomposition is occurring, the chemistry becomes more complex, and the total radical pool

Table 6. Prior Rate Coefficients and Prior and Posterior Rate Constant Values Evaluated at 950 K[a]

		Prior rate coefficients							rate constants at 950 K		
n	name	log 10 A^b			b^b	E/R (K)^b			log 10 k^{*c}	log 10 k	k^*/k^c
	Title Reactions										
633	C_4H_{10} + H ↔ pC_4H_9 + H_2	5.96	±	0.48	2.54	3404	±	681	11.94	11.97	0.93
634	C_4H_{10}+H ↔ sC_4H_9 + H_2	6.38	±	0.48	2.40	2252	±	450	12.34	12.50	0.69
	$(k_p)/(k_s)$	−0.42	±	0.67	0.14	1151	±	816			
643	C_4H_{10} + CH_3 ↔ pC_4H_9 + CH_4	−0.0443	±	0.48	3.65	3604	±	721	9.43	9.18	1.78
644	C_4H_{10} + CH_3 ↔ sC_4H_9 + CH_4	0.48	±	0.48	3.46	2761	±	552	9.79	9.52	1.87
	$(k_p)/(k_s)$	−0.52	±	0.67	0.19	843	±	908			
	C−C Bond Fission Reactions										
631	nC_3H_7+CH_3(+M)↔C_4H_{10}(+M)	14.29	±	0.30	−0.32	0		–	13.50	13.33	1.46
	(k_0)	61.43	±	0.30	−13.24	3023		–	20.78	20.62	1.46
632	$2C_2H_5$(+M)↔C_4H_{10}(+M)	14.27	±	0.30	−0.50	0		–	12.73	12.79	0.88
	(k_0)	61.42	±	0.30	−13.42	3023		–	20.02	20.07	0.88
	Reactions of Toluene										
673	$C_6H_5CH_3$ + H ↔ $C_6H_5CH_2$ + H_2	14.10	±	0.30	0.00	4211	±	674	11.74	12.18	0.37
674	$C_6H_5CH_3$ + H ↔ C_6H_6 + CH_3	6.29	±	0.30	2.17	2097	±	419	11.61	11.79	0.66
676	$C_6H_5CH_3$ + CH_3 ↔ $C_6H_5CH_2$ + CH_4	11.50	±	0.30	0.00	4786	±	670	9.47	9.31	1.44
680	$C_6H_5CH_2$ + H(+M) ↔ $C_6H_5CH_3$ (+M)	14.00	±	0.30	0.00	0		–	14.00	14.00	1.00
	(k_0)	103.04	±	0.30	−24.63	7350		–	26.33	26.33	1.00
805	$C_6H_5CH_2$ + CH_3 ↔ $C_6H_5C_2H_5$	18.91	±	0.30	−1.81	976	±	195	13.01	13.07	0.88
820	$2C_6H_5CH_2$ ↔ $(C_6H_5CH_2)_2$	20.89	±	0.30	−2.67	672		–	12.58	12.64	0.87
	Reactions of Methyl and Ethyl										
91	CH_3+H(+M)↔CH_4(+M)	16.10	±	0.30	−0.63	193		–	14.10	14.14	0.91
	(k_0)	33.39	±	0.30	−4.76	1229		–	18.62	18.66	0.91
107	$2CH_3$(+M) ↔ C_2H_6(+M)	16.33	±	0.30	−0.97	312		–	13.23	13.30	0.86
	(k_0)	50.24	±	0.30	−9.67	3134		–	19.95	20.01	0.86
108	$2CH_3$ ↔ H + C_2H_5	12.70	±	0.70	0.10	5340	±	1068	10.18	10.55	0.42
252	C_2H_4 + H(+M) ↔ C_2H_5(+M)	9.14	±	0.48	1.46	683		–	13.38	13.18	1.57
	(k_0)	39.31	±	0.48	−6.64	2906		–	18.39	18.20	1.57
264	C_2H_6 + CH_3 ↔ C_2H_5 + CH_4	5.36	±	0.70	2.00	4635		–	9.23	9.19	1.08
279	C_2H_5 + CH_3(+M) ↔ C_3H_8(+M)	14.69	±	0.48	−0.50	0		–	13.48	13.20	1.91
	(k_0)	61.92	±	0.48	−13.42	3023		–	20.86	20.58	1.91
282	C_2H_6 + H ↔ C_2H_5 + H_2	8.06	±	0.30	1.90	3793	±	683	12.06	11.98	1.19
286	C_2H_6 + CH_3 ↔ C_2H_5 + CH_4	6.79	±	0.30	1.74	5264	±	684	9.65	9.56	1.22
	Other Secondary Chemistry										
362	C_3H_6 + H ↔ C_2H_4 + CH_3	21.90	±	0.30	−2.39	5632	±	676	12.15	12.21	0.87
363	C_3H_6 + H ↔ aC_3H_5 + H_2	5.24	±	0.30	2.50	1254		–	12.08	12.11	0.93
553	1-C_4H_8 + H(+M) ↔ pC_4H_9(+M)	9.08	±	0.48	1.32	528		–	12.62	12.78	0.69
	(k_0)	34.75	±	0.48	−5.34	2412		–	17.59	17.76	0.69
554	1-C_4H_8 + H(+M) ↔ sC_4H_9(+M)	8.82	±	0.48	1.39	−341		–	12.78	13.11	0.47
	(k_0)	38.64	±	0.48	−6.11	1252		–	19.54	19.86	0.47
565	2-C_4H_8 + H(+M) ↔ sC_4H_9(+M)	8.45	±	0.48	1.49	329		–	12.59	12.75	0.70
	(k_0)	38.26	±	0.48	−6.01	1922		–	19.34	19.50	0.70
573	iC_4H_8 + H ↔ iC_4H_7 + H_2	6.08	±	0.48	2.54	3406	±	681	12.04	12.09	0.90
574	iC_4H_8 + H ↔ C_3H_6 + CH_3	21.90	±	0.48	−2.39	5632	±	1126	12.25	12.21	1.10
582	C_2H_4 + C_2H_5 ↔ pC_4H_9	2.45	±	0.48	2.84	2591	±	518	9.93	9.73	1.61
592	C_3H_6 + CH_3(+M) ↔ sC_4H_9(+M)	4.08	±	0.30	2.39	3730		–	9.77	9.50	1.85
	(k_0)	21.21	±	0.30	−1.88	−173		–	15.97	15.70	1.85
604	sC_4H_9 + CH_3 ↔ C_2H_4 + 1-C_4H_8	14.34	±	0.70	−0.68	0		–	12.37	12.32	1.12
869	pC_4H_9 + CH_3 ↔ nC_5H_{12}	14.29	±	0.30	−0.32	0		–	13.28	13.33	1.00
870	sC_4H_9 + CH_3 ↔ iC_5H_{12}	15.15	±	0.30	−0.68	0		–	13.14	13.12	1.00

[a] All uncertainties are 2σ. [b] $k = AT^b \exp(ER^{-1}T^{-1})$. Logarithmic uncertainty $\sigma = 1/2 \ln f$. See Table 5 for uncertainty factors. [c] Starred quantities refer to the Posterior model, while unstarred quantities refer to the Prior model. Parameters without listed uncertainties were inactive.

increases. A consequence is that the action of the inhibitor is partially overcome, the importance of free radical chains increases, and it becomes more difficult to correctly determine the overall chain length and thus absolute product amounts. These conditions are unsurprisingly the most difficult to predict.

H atoms attack both *n*-butane and the toluene inhibitor. An unequivocal marker for H atoms is the formation of benzene that occurs via displacement of methyl from toluene. In the HME systems, where a large fraction of the H atoms are directly generated from the precursor, absolute and relative amounts of benzene are well-predicted (Figure 8). However, in the *t*BPO systems with low starting concentrations of *n*-butane (mixtures F and G), the observed production of benzene is significantly larger than predicted by the model (Figure 7). Modeled H atom production in these systems is due to secondary chemistry (e.g., decomposition of ethyl radicals). Large changes to the rate constants for the known secondary chemistry would result in problems in the fits for the other mixtures. Our interpretation of the "excess" benzene in these experiments, where the production rate of H atoms from nominal sources is low, is that small quantities of additional H arise from unknown sources. The effect of this possibility on our results was explored by adding to the Posterior model an artificial source of H at the 1 ppm level, which results in an approximate match to the experimental benzene production. Selected results from this augmented model are shown in Figure 9 and compared with the unmodified Posterior model. For present purposes, the important observation is that the required amount of H has little impact on absolute and relative amounts of ethene and propene and thus does not significantly affect derived rate constants for the title reactions.

5.4. Recommended Rate Constants for Abstraction of H from *n*-Butane.

Rate parameters derived for the title and other active reactions using the constraints of Tables 2 and 3 are given in Tables 5 and 6. Parameters of the Prior and Posterior models are summarized therein, together with changes in the uncertainties and a comparison of rate constants at 950 K.

Rate expressions are given in the standard modified Arrhenius form $k = AT^b \exp(-E/T)$. The present data cover only a short temperature range and therefore yield values of b only when coupled with lower-temperature results. The values of b used in JetSurf 2 for the title reactions are equal to those given by Tsang in his review and evaluation of propane combustion chemistry.[1] For attack of H atoms on the primary and secondary hydrogens of propane, Tsang employed b_p = 2.54 and b_s = 2.40, respectively. For comparison, these are only modestly different from the values of b_p = 2.45 and b_s = 2.12 that we have derived from a fit to the theoretical results of Kerkeni and Clary,[69] who investigated the kinetics of the H + propane reaction from 200 to 2000 K, including tunneling, using combined quantum chemical and quantum dynamics calculations. For attack of CH_3 radicals on the primary and secondary hydrogens of propane, Tsang employed b_p = 3.65 and b_s = 3.46, respectively. In two separate trials, we also explored fits using equal values of b for $k_s(CH_3)$ and $k_p(CH_3)$, using $b_p = b_s = 2$ in one instance and in the other taking both values as 3. Such variations led to absolute rate constants for the title reactions that differed by less than 40% at temperatures equal or greater than those of the present study. At 300 K, changes were up to a factor of 2.5. Branching ratios for k_s/k_p were affected by less than 10% throughout. In part, these results are indicative that the values of A, b, and E are highly correlated, so that only in the case of gross errors do changes in b significantly affect the ability to fit rate constants within the current experimental uncertainties. After consideration, we have elected to fix values of b at those used in the Prior model.

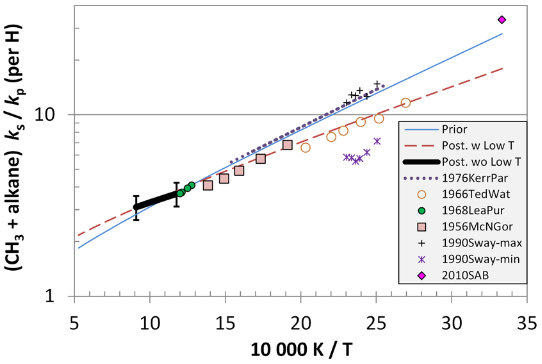

Figure 10. Relative rate data for abstraction of primary and secondary hydrogens of *n*-alkanes by methyl radicals. Experimental data: 1956McNGor[37] (*n*-butane); 1966TedWat[38] (*n*-butane); 1968LeaPur[39] (propane); 1990Sway[40] (various hydrocarbons). Evaluation (generic alkanes): 1976KerrPar.[33] Reference value used in TST-based fits: 2010Sab[71]. The dashed and heavy solid lines indicate Posterior model fits to the current data with and without inclusion of the low-temperature literature data as targets; error limits are 2σ. The light solid line indicates the Prior model. See text.

Abstraction of Hydrogen by CH_3 Radicals. Figure 10 summarizes the current results and selected data from the literature on the relative rate of abstraction of primary and secondary hydrogens of *n*-butane by methyl radicals. The minimum and maximum values from the Sway data were derived by us as discussed in Section 5.2.3. The present analysis indicates a weaker temperature dependence of $k_s(CH_3)/k_p(CH_3)$ than the generally accepted value given by Kerr and Parsonage.[33] The difference appears to result primarily from the earlier misinterpretation of the Tedder and Watson[38] results as absolute rather than per H rate constants (see Section 5.2.3). This error has been propagated in subsequent reviews and also in the reference training data used in recent TST-based fits.[71] The largest impact occurs at lower temperatures, where the difference is a factor of 1.5. It would be desirable to confirm the result of Tedder and Watson, but as it stands, there is good agreement in data spanning 370 to 1030 K. On a per H basis, the relative abstraction rates of primary and secondary hydrogens for *n*-butane can be expressed as

$$k_p(CH_3)/k_s(CH_3) = 10^{(-0.817 \pm 0.062)} T^{0.19}$$

$$\exp[-(626 \pm 117)\ \mathrm{K}/T],$$

$$370\ \mathrm{K\ to\ 2000\ K}; \quad \text{per H basis}$$

The estimated uncertainty (2σ) is about 25% at 370 K, decreasing to 15% near 1000 K and then rising to 25% at 2000 K. Note that in the absence of further information, this expression is a reasonable generic estimate for all *n*-alkanes and can be extended to the primary and secondary sites of branched alkanes and related species in most cases. Polar substituents close to the abstraction site are likely to result in substantial deviations, however, and the impact of nearby highly branched structures is uncertain.

With respect to absolute rate constants, experimental and recommended values of $k_p(CH_3)$ for various alkanes are summarized in Figure 11. At high temperatures, the only inconsistent data are the rate constants of Møller et al.[72] for CH_3 + ethane, obtained using optical absorption techniques for methyl radicals. These appear to be too large and are in poor agreement with the other data. It is possible to achieve compatibility of the high- and low-temperature results only if one posits significant curvature in the rate expression, such as might be induced by tunneling. Previous reviews[33,73] have likewise noted difficulties in reconciling the low- and high-temperature results. Our modified Arrhenius fits of the form $k = AT^b \exp(-E/T)$ utilize the b values of Tsang, which are near 3.5. Assuming similarity in the k_p for the normal alkanes, this

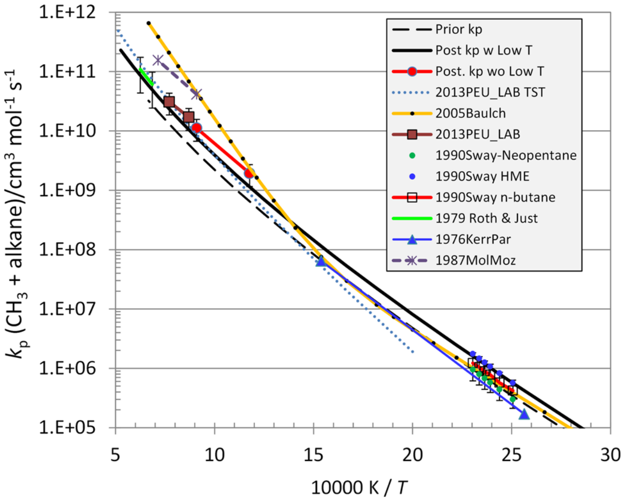

Figure 11. Absolute rate constants for abstraction of primary hydrogens of *n*-alkanes by methyl radicals. Experimental data: 2013Peu[41] (ethane); 1987MolMoz[72] (ethane); 1979Roth&Just[42] (ethane); and 1990Sway[40] (various hydrocarbons). Evaluations:1976KerrPar[33] (generic alkanes), 2005Baulch[73] (ethane). The Posterior model fits to the current data for *n*-butane with and without inclusion of the low-temperature literature data as targets are as indicated; the light dashed line indicates the Prior model, and the dotted line shows the TST model (for ethane) of Peukert et al.[41]

leads to acceptable if not fully satisfying agreement between the data of Sway, the present results, and the H-atom ARAS measurements. As noted earlier, we explored fits using other values of *b*, but this did not lead to obviously better results.

Previous recommendations deviate from the present analysis in a number of respects. In the combustion-relevant regime, the present values are about a factor of two larger than the 1988 recommendation of Tsang[1] of k_p for propane. The 2005 values of Baulch et al.[73] for $CH_3 + C_2H_6$ show fair agreement at lower temperatures but increasingly deviate at high temperatures and are a factor of 5 larger at 1200 K. The 2013 TST fit of Peukert et al.[41] for $CH_3 + C_2H_6$ is reasonably similar to the present recommendation at higher temperatures but is a factor of 5 lower at 500 K and extrapolates poorly to the lower temperature k_p results of Sway. The disagreement of the experiment with the TST result could indicate an issue with the data of Sway at lower temperatures, but there are no obvious indications of error in his results. At present, we think that the absolute rate constants are better defined at higher temperatures, where rate constants are larger and have been determined with modern methods. The extrapolation to lower temperatures remains less certain, and it would be desirable to remeasure rate constants in that regime with newer techniques.

Recommended generic values of $k_p(CH_3)$ and $k_s(CH_3)$ are given below on a per H basis.

$$k_p(\mathrm{CH_3})/\mathrm{cm^3\ mol^{-1}\ s^{-1}} = 10^{(-0.55\pm0.13)}T^{3.65}$$
$$\exp[-(3650 \pm 156)\ \mathrm{K}/T),$$
$$400\ \mathrm{K\ to\ 2000\ K;\ per\ H\ basis}$$

$$k_s(\mathrm{CH_3})/\mathrm{cm^3\ mol^{-1}\ s^{-1}} = 10^{(0.27\pm0.13)}T^{3.46}$$
$$\exp[-(3024 \pm 198)\ \mathrm{K}/T),$$
$$400\ \mathrm{K\ to\ 2000\ K;\ \ per\ H\ basis}$$

These are based on our optimized fit for the *n*-butane system. Although derived specifically for *n*-alkanes, the extension to branched hydrocarbons and related species is reasonable in most cases. The listed uncertainties are the 2σ statistical values from our analysis. Estimated expanded uncertainties (2σ) for the lower *n*-alkanes are a factor of 1.6 between 700 and 1600 K. At 400 K, the uncertainty in the absolute values increases to as much as a factor of four, although the relative rate constants, $k_p(CH_3)/k_s(CH_3)$, should still be reliable. Small deviations from the generic values may well arise in the hydrocarbon series, but these are currently unresolved. Theoretical studies or experiments involving direct competitions may be useful to better discern trends and differences for specific hydrocarbons and hydrocarbon classes.

Abstraction of Hydrogen by H Atoms. Data on the relative rates of abstraction of primary and secondary hydrogens from alkanes by H atoms are summarized in Figure 12. The present results are in very good agreement with the data from experiments at lower temperatures (discussed in Section 5.2.3). The fit of the Posterior model is very similar to the 1988 recommendation of Tsang[1] for propane but deviates by a factor of 1.5 to 2.5 from the current value in JetSurF 2, the 2005 theoretical results of Kerkeni and Clarey,[69] and the 1991 assessment of Cohen.[2] The theoretical values derived by Carstensen and Dean[74] in 2009 and Peukert et al.[75] in 2015 are in good agreement but fall outside the 2σ error limits of the present experiments. As noted earlier, the values derived by Nicolas and Vaghjiani are in poor accord. On a per H basis, the relative abstraction rates of primary and secondary hydrogens for *n*-butane can be expressed as

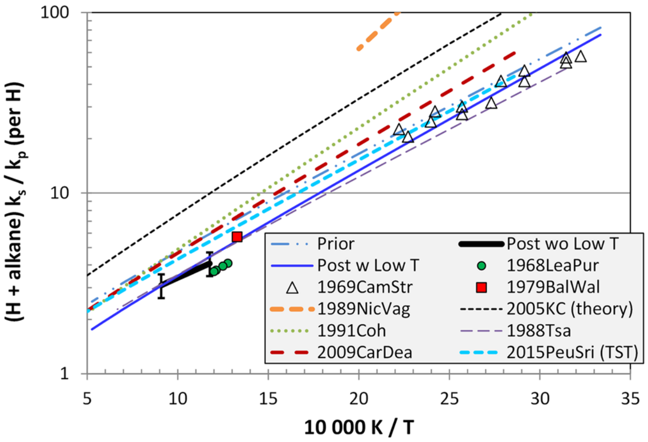

Figure 12. Relative rate data for abstraction of primary and secondary hydrogens of *n*-alkanes by H atoms. Experimental data: 1968LeaPur[39] (propane), 1969CamStr[48] (propane), 1979BalWal[43] (generic C2–C5 alkanes), and 1989NiCVag[54] (*n*-butane). Theory: 2005KC[69] (propane), 2009CarDea[74] (*n*-butane), and 2015PeuSri[75] (*n*-butane). Evaluations: 1988Tsa[1] (propane) and 1991Coh[2] (*n*-butane). Values from the Prior and Posterior models with and without inclusion of the low temperature literature data are as indicated. Error limits are 2σ.

$$k_p(\mathrm{H})/k_s(\mathrm{H}) = 10^{(-0.421\pm0.066)}T^{0.14}$$
$$\exp[-(1246 \pm 141)\ \mathrm{K}/T),$$
$$300\ \mathrm{K\ to\ 2000\ K;\ per\ H\ basis}$$

In the absence of further information, this expression is a reasonable generic estimate for all *n*-alkanes and can be extended to branched hydrocarbons and related species in most cases, albeit with increased uncertainties. Nearby polar substituents are expected to cause substantial deviations.

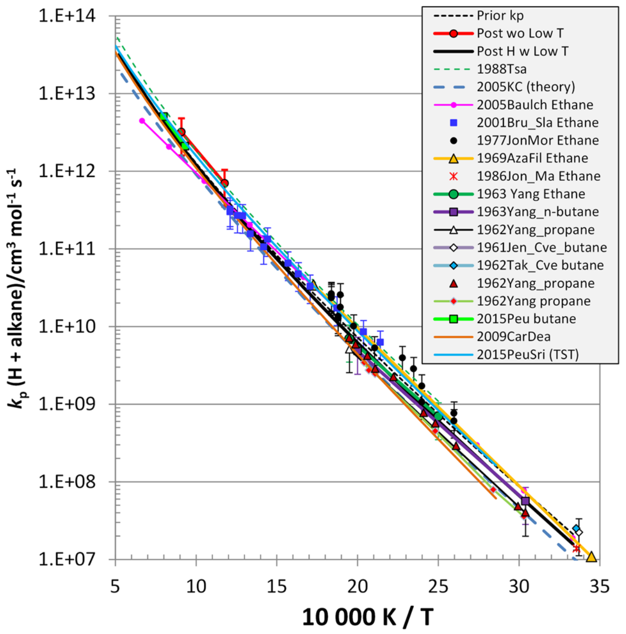

Figure 13. Absolute rate constants for abstraction of primary hydrogens of *n*-alkanes by H atoms. Absolute experimental data: 1969AzaFil[67] (ethane), 1977JonMor[65] (ethane), 1986JonMa[66] (ethane), and 2001BruSla[64] (ethane). Relative Rate experimental data: 1961JenCve[55] (*n*-butane), 1962TakCve[76] (*n*-butane), 1963YangA[57] (ethane, *n*-butane), 1963YangB[56] (propane), and 2015PeuSri[75] (*n*-butane: k_{total} converted to k_p using our k_s/k_p recommendation). Evaluations: 1988Tsa[1] (propane) and 2005Bau (ethane). Theory: 2005KC[69] (propane), 2009CarDea[74] (*n*-butane), and 2015PeuSri[75] (*n*-butane). The Posterior model fits to the current data for *n*-butane with and without inclusion of the low temperature literature data as targets are as indicated; the light dashed line indicates the Prior model.

Experimental and recommended absolute values of $k_p(\mathrm{H})$ for various alkanes are summarized in Figure 13. The present data and analysis results in only small changes to the fit of the Prior model. Figure 13 shows there are systematic differences in the $k_p(\mathrm{H})$ results from the various types of studies. Rate constants from the flow discharge/mass spectrometer system of Jones et al.[65] are systematically larger than values derived by combining direct measurements of H addition to olefins with experimental results that compare the olefin addition rates with abstraction rates from alkanes (see also Section 5.2.3). The direct study of H + ethane by Bryukov et al.[64] using a discharge flow/resonance fluorescence technique results in good agreement with the present fit over the temperature range of overlap but exhibits a weaker temperature dependence and does not extrapolate well to more recent measurements at higher temperatures. Despite the various disagreements, all of the data can be fit within a factor of about 1.5 over the temperature range of 300 to 1250 K. Peukert et al.[75] have recently used D atom ARAS to directly measure the overall rate constant of the D + *n*-butane reaction at temperatures of 1074 to 1253 K and have argued on the basis of high-level calculations that k_H/k_D is very close to 1, so that these data also closely approximate the kinetics of H + *n*-butane. Although not used in our derivation, conversion of the experimental measurements of Peukert et al. to values of $k_p(\mathrm{H})$ using our recommendation for $k_s(\mathrm{H})/k_p(\mathrm{H})$ leads to excellent agreement, within 13%, with the presently derived $k_p(\mathrm{H})$ values (deviations in the derived values for $k_s(\mathrm{H})$ are about 25%). Compared with their theoretical predictions reported in the same paper, the present evaluation agrees within about 25% for $k_p(\mathrm{H})$ and 40% for $k_s(\mathrm{H})$ at the temperatures of their experiments; agreement is similar over the full 300 to 2000 K temperature range, with maximum deviations in $k_p(\mathrm{H})$ and $k_s(\mathrm{H})$ of 30% and 40%, respectively.

Our recommended generic values of $k_p(\mathrm{H})$ and $k_s(\mathrm{H})$ are given below on a per H basis.

$$k_p(\mathrm{H})/\mathrm{cm^3\ mol^{-1}\ s^{-1}} = 10^{(5.20\pm0.16)}T^{2.54}$$
$$\exp[-(3511 \pm 152)\ \mathrm{K}/T);$$
$$300\ \mathrm{K\ to\ 2000\ K;\ \ per\ H\ basis}$$

$$k_s(\mathrm{H})/\mathrm{cm^3\ mol^{-1}\ s^{-1}} = 10^{(5.62\pm0.16)}T^{2.40}$$
$$\exp[-(2265 \pm 183)\ \mathrm{K}/T),$$
$$300\ \mathrm{K\ to\ 2000\ K;\ \ per\ H\ basis}$$

These expressions and statistical uncertainties (2σ) are based on our optimized fit and pertain specifically to *n*-alkanes. They can, however, be reasonably extended to branched hydrocarbons and related species in most cases. As per previous discussion, nearby polar substituents are expected to cause substantial deviations.

With regard to the absolute rate constants, the present evaluation agrees very well with the recommendations of Peukert et al.[75] and Carstensen and Dean,[74] and the new experimental data provide further confirmation of the absolute rate constant. A more important contribution of the present experiments, however, is the reliable measurement of the k_s/k_p branching ratio at temperatures higher than previously reported. This branching ratio significantly impacts olefin fractions in H atom induced breakdown of hydrocarbon fuels, and the product ratios will propagate through the subsequent chemistry. The primary advantage of the present absolute rate recommendations is that they incorporate an improved estimate of the $k_s(\mathrm{H})/k_p(\mathrm{H})$ ratio and its temperature dependence.

6. SUMMARY AND CONCLUSIONS

The present work presents a combined experimental and modeling study of the kinetics of the reactions of H atoms and CH_3 radicals with *n*-butane. Experiments have been carried out between 900 and 1150 K and pressures from 150 to 300 kPa. By generating the radicals of interest in separate experiments under well-defined conditions, we have been able to separate the kinetics of the two processes despite the fact that both radicals are present in both systems. A mathematical design algorithm has been applied to select the optimum conditions under which the kinetics can be disentangled. In conjunction with postshock product analyses, detailed chemical modeling, and the use of polynomial chaos expansion techniques, the absolute and relative rate constants for attack of H and CH_3 on the primary and secondary hydrogens of *n*-butane have been determined. Of particular interest are the relative rate constants, which have been determined at temperatures higher than heretofore examined. The abstraction ratios, a determinant of the species mass flow in practical systems, is defined with high precision by the present data. Results at lower temperatures from the literature have been reviewed and some problems identified. The current results are combined with re-evaluated literature data and updated rate expressions covering 300 to 2000 K for H atoms and 400 K to 2000 K for methyl radicals are provided. Taken on a per H basis, these rate expressions should be transferrable with minimal error to unstudied *n*-alkanes for use in combustion and pyrolysis models.

In addition to determining the kinetics of the title reactions, the present data show that C−H bond scission channels in the decomposition of butyl radicals are less important by an order of magnitude than currently indicated by the commonly used combustion model JetSurf 2. This is of significant interest as butyl radicals are important intermediates produced in the fragmentation of a wide variety of existing and future fuels. Further, because data on small molecules are typically used to extrapolate to larger species, this can impact models of the initial olefin and radical pool for many systems. This, in turn, will propagate through the subsequent chemistries associated with ignition, combustion, and formation of byproducts. Detailed models and chemical understanding cannot be reliable if the initial fuel fragmentation patterns are incorrect. We note in particular that branching ratios for elementary reactions are difficult to obtain reliably from global experiments or calculated a priori with accuracy similar to high-quality experiments.[15−17,77] Reference studies specifically designed to probe the reactions and carried out under well-defined conditions with detailed product monitoring, such as those reported here, are required. At this time, the shock tube methodology is probably the only way of obtaining precise and accurate information at high temperatures.

■ ASSOCIATED CONTENT

Ⓢ Supporting Information

Product data from shock tube experiments with mixtures A through G, sensitivity coefficient plots for selected mixtures and experimental observables, CHEMKIN format text files of the Prior and Posterior models, and the CHEMKIN Interpreter Output File. The Supporting Information is available free of charge on the ACS Publications website at DOI: 10.1021/acs.jpca.5b01004.

■ AUTHOR INFORMATION

Corresponding Author

*E-mail: jeffrey.manion@nist.gov. Tel: 301-975-3188.

Notes

The authors declare no competing financial interest.

Disclaimer: certain commercial materials and equipment are identified in this paper in order to specify adequately the experimental procedure. In no case does such identification imply recommendation of endorsement by the National Institute of Standards and Technology, nor does it imply that the material or equipment is necessarily the best available for the purpose.

■ REFERENCES

(1) Tsang, W. Chemical Kinetic Data-Base for Combustion Chemistry 0.3. Propane. *J. Phys. Chem. Ref. Data* **1988**, *17*, 887−952.

(2) Cohen, N. The Use of Transition-State Theory to Extrapolate Rate Coefficients for Reactions of H-Atoms with Alkanes. *Int. J. Chem. Kinet.* **1991**, *23*, 683−700.

(3) Wang, H.; Dames, E.; Sirjean, B.; Sheen, D. A.; Tangko, R.; Violi, A.; Lai, J. Y. W.; Egolfopoulos, F. N.; Davidson, D. F.; Hanson, R. K.; et al. *JetSurF*, version 2.0. A High-Temperature Chemical Kinetic Model of n-alkane (up to n-dodecane), cyclohexane, and methyl-, ethyl-, n-propyl, and n-butyl-cyclohexane Oxidation at High Temperatures, 2010. http://melchior.usc.edu/JetSurF/JetSurF2.0 (accessed Sept 19, 2010).

(4) Sheen, D. A.; Manion, J. A. Kinetics of the Reactions of H and CH_3 Radicals with *n*-Butane: An Experimental Design Study Using Reaction Network Analysis. *J. Phys. Chem. A* **2014**, *118*, 4929−4941.

(5) Awan, I. A.; McGivern, W. S.; Tsang, W.; Manion, J. A. Decomposition and Isomerization of 5-Methylhex-1-yl Radical. *J. Phys. Chem. A* **2010**, *114*, 7832−7846.

(6) Tsang, W. Comparative-Rate Single-Pulse Shock Tube Studies on the Thermal Stability of Polyatomic Molecules. In *Shock Waves in Chemistry*, Lifshitz, A., Ed.; Marcel Decker: New York and Basel, 1981.

(7) Awan, I. A.; Burgess, D. R., Jr.; Tsang, W.; Manion, J. A. Standard Reactions for Comparative Rate Studies: Experiments on the Dehydrochlorination Reactions of 2-Chloropropane, Chlorocyclopentane and Chlorocyclohexane. *Int. J. Chem. Kinet.* **2012**, *44*, 351−368.

(8) Raley, J. H.; Rust, F. F.; Vaughan, W. E. Decompositions of Di-*t*-Alkyl Peroxides. 1. Kinetics. *J. Am. Chem. Soc.* **1948**, *70*, 88−94.

(9) Manion, J. A.; Huie, R. E.; Levin, R. D.; Burgess, D. R., Jr.; Orkin, V. L.; Tsang, W.; McGivern, W. S.; Hudgens, J. W.; Knyazev, V. D.; Atkinson, D. B.; et al. NIST Chemical Kinetics Database, NIST Standard Reference Database 17, Version 7.0 (Web Version), Release 1.6.8, Data version 2013.03, National Institute of Standards and Technology: Gaithersburg, MD, 2013, pp 20899−28320 (http://kinetics.nist.gov/).

(10) Lewis, D. K. Di-*tert*-Butyl Peroxide Decomposition Behind Shock-Waves. *Can. J. Chem.* **1976**, *54*, 581−585.

(11) Batt, L.; Hisham, M. W. M.; Mackay, M. Decomposition of the *tert*-Butoxy Radical. II. Studies over the Temperature-Range 303−393 K. *Int. J. Chem. Kinet.* **1989**, *21*, 535−546.

(12) Batt, L.; Robinson, G. N. Decomposition of the *tert*-Butoxy Radical. I. Studies over the Temperature-Range 402−443-K. *Int. J. Chem. Kinet.* **1987**, *19*, 391−400.

(13) Batt, L.; Robinson, G. N. Arrhenius Parameters for the Decomposition of the *tert*-Butoxy Radical. *Int. J. Chem. Kinet.* **1982**, *14*, 1053−1055.

(14) Tsang, W. Thermal Decomposition of Hexamethylethane 2,2,3-Trimethylbutane and Neopentane in a Single-Pulse Shock Tube. *J. Chem. Phys.* **1966**, *44*, 4283−4295.

(15) Manion, J. A.; Awan, I. A. The Decomposition of 2-Pentyl and 3-Pentyl Radicals. *Proc. Combust. Inst.* **2013**, *34*, 537−545.

(16) Comandini, A.; Awan, I. A.; Manion, J. A. Thermal Decomposition of 1-Pentyl Radicals at High Pressures and Temperatures. *Chem. Phys. Lett.* **2012**, *552*, 20−26.

(17) Awan, I. A.; Burgess, D. R., Jr.; Manion, J. A. Pressure Dependence and Branching Ratios in the Decomposition of 1-Pentyl Radicals: Shock Tube Experiments and Master Equation Modeling. *J. Phys. Chem. A* **2012**, *116*, 2895−2910.

(18) Yamauchi, N.; Miyoshi, A.; Kosaka, K.; Koshi, M.; Matsui, N. Thermal Decomposition and Isomerization Processes of Alkyl Radicals. *J. Phys. Chem. A* **1999**, *103*, 2723−2733.

(19) Miller, J. A.; Klippenstein, S. J. Dissociation of Propyl Radicals and Other Reactions on a C_3H_7 Potential. *J. Phys. Chem. A* **2013**, *117*, 2718−2727.

(20) Davis, A. C.; Francisco, J. S. Ab Initio Study of Hydrogen Migration across *n*-Alkyl Radicals. *J. Phys. Chem. A* **2011**, *115*, 2966−2977.

(21) Hayes, C. J.; Burgess, D. R., Jr. Kinetic Barriers of H-Atom Transfer Reactions in Alkyl, Allylic, and Oxoallylic Radicals as

Calculated by Composite Ab Initio Methods. *J. Phys. Chem. A* **2009**, *113*, 2473−2482 DOI: 10.1021/jp810147z.

(22) Robaugh, D.; Tsang, W. Mechanism and Rate of Hydrogen Atom Attack on Toluene at High-Temperatures. *J. Phys. Chem.* **1986**, *90*, 4159−4163.

(23) Sheen, D. A.; Rosado-Reyes, C. M.; Tsang, W. Kinetics of H Atom Attack on Unsaturated Hydrocarbons using Spectral Uncertainty Propagation and Minimization Techniques. *Proc. Combust. Inst.* **2013**, *34*, 527−536.

(24) Brown, P. N.; Byrne, G. D.; Hindmarsh, A. C. Vode: A Variable-Coefficient Ode Solver. *Siam Journal on Scientific and Statistical Computing* **1989**, *10*, 1038−1051.

(25) Kee, R. J.; Rupley, F. M.; Miller, J. A. *CHEMKIN-II: A FORTRAN Chemical Kinetics Package for the Analysis of Gas-Phase Chemical Kinetics*; SAND89-8009; Sandia National Laboratories: Albequerque, NM, 1989.

(26) Sheen, D. A.; Wang, H. The Method of Uncertainty Quantification and Minimization using Polynomial Chaos Expansions. *Combust. Flame* **2011**, *158*, 2358−2374.

(27) More, J.; Garbow, B.; Hillstrom, K. *Minpack*. http://netlib.org/minpack/index.html (accessed March 6, 2012).

(28) Frenklach, M. Systematic Optimization of a Detailed Kinetic-Model Using a Methane Ignition Example. *Combust. Flame* **1984**, *58*, 69−72.

(29) Frenklach, M.; Wang, H.; Rabinowitz, M. J. Optimization and Analysis of Large Chemical Kinetic Mechanisms Using the Solution Mapping Method: Combustion of Methane. *Prog. Energy Combust. Sci.* **1992**, *18*, 47−73.

(30) Davis, S. G.; Mhadeshwar, A. B.; Vlachos, D. G.; Wang, H. A New Approach to Response Surface Development for Detailed Gas-Phase and Surface Reaction Kinetic Model Optimization. *Int. J. Chem. Kinet.* **2004**, *36*, 94−106.

(31) Knyazev, V. D.; Slagle, I. R. Unimolecular Decomposition of *n*-C4H9 and *iso*-C4H9 Radicals. *J. Phys. Chem.* **1996**, *100*, 5318−5328.

(32) Knyazev, V. D.; Dubinsky, I. A.; Slagle, I. R.; Gutman, D. Experimental and Theoretical-Study of the *sec*-C_4H_9 ↔ CH_3 + C_3H_6 Reaction. *J. Phys. Chem.* **1994**, *98*, 11099−11108.

(33) Kerr, J. A.; Parsonage, M. J. *Evaluated Kinetic Data on Gas Phase Hydrogen Transfer Reactions of Methyl Radicals*; Butterworth: London, 1976.

(34) Jackson, W. M.; McNesby, J. R. Photolysis of Acetone-D_6 in the Presence of Propane-2,2-D_2. Decomposition of *n*-Propyl Radical. *J. Am. Chem. Soc.* **1961**, *83*, 4891−4896.

(35) Jackson, W. M.; Darwent, B. D.; McNesby, J. R. Reaction of Methyl-D_3 Radicals with Isobutane, Isobutane-2-D, and Propane. *J. Chem. Phys.* **1962**, *37*, 1610−1615.

(36) Benson, S. W. *Thermochemical Kinetics*, 2nd ed.; Wiley: New York, 1976.

(37) McNesby, J. R.; Gordon, A. S. Photolysis of Acetone-D_6 in the presence of normal-Butane and normal-Butane-2,2,3,3-D_4: A Study of the Abstraction of Primary and Secondary Hydorgen by Methyl Radicals. *J. Am. Chem. Soc.* **1956**, *78*, 3570−3573.

(38) Tedder, J. M.; Watson, R. A. Free-Radical Substitution in Aliphatic Compounds. Part XVI. Reaction of Methyl Radicals with N-Butane. *J. Chem. Soc. B* **1966**, 1069−1071.

(39) Leathard, D. A.; Purnell, J. H. Self-Inhibited Pyrolysis of Propane at Small Extents of Reaction. *Proc. R. Soc. London, Ser. A* **1968**, *305*, 517−540.

(40) Sway, M. I. Kinetics of Abstraction Reactions of Methyl Radicals with Alkanes in Gas-Phase. *Indian J. Chem., Sect. A: Inorg., Bio-Inorg., Phys., Theor. Anal. Chem.* **1990**, *29*, 748−752.

(41) Peukert, S. L.; Labbe, N. J.; Sivaramakrishnan, R.; Michael, J. V. Direct Measurements of Rate Constants for the Reactions of CH_3 Radicals with C_2H_6, C_2H_4, and C_2H_2 at High Temperatures. *J. Phys. Chem. A* **2013**, *117*, 10228−10238.

(42) Roth, P.; Just, T. Measurements on the High-Temperature Pyrolysis of Ethane. *Ber. Bunsen-Ges.* **1979**, *83*, 577−583.

(43) Baldwin, R. R.; Walker, R. W. Rate Constants for Hydrogen + Oxygen System, and for H-Atoms and OH Radicals + Alkanes. *J. Chem. Soc., Faraday Trans. I* **1979**, *75*, 140−154.

(44) Baker, R. R.; Baldwin, R. R.; Walker, R. W. Addition of C_3H_8, Normal and i-C_4H_{10} to Slowly Reacting Mixtures of Hydrogen and Oxygen at 480 Degrees C: Reactions of H and OH Radicals with Additive. *Trans. Faraday Soc.* **1970**, *66*, 2812.

(45) Lede, J.; Villermaux, J. Measurement of the Rate Constant for Reaction of Hydrogen Atoms with Ethane and Propane in Tubular and Perfectly Stirred Reactors. *Can. J. Chem.* **1978**, *56*, 392−401.

(46) Lede, J.; Villermaux, J. Measurement of Kinetic Constants of Very Reactive Species in Flow Systems. 1. Tubular Reactor in Laminar Flow. *J. Chim. Phys. Phys.-Chim. Biol.* **1977**, *74*, 459−467.

(47) Marshall, R. M.; Purnell, H.; Sheppard, A. Reaction of Hydrogen-Atoms with Propane in the Temperature-Range 298−534-K. *J. Chem. Soc., Faraday Trans. I* **1984**, *80*, 2999−3009.

(48) Campbell, J. M.; Strausz, O. P.; Gunning, H. E. Reaction of Hydrogen Atoms with Propane: Relative Arrhenius Parameters for Attack on 1 and 2 Positions. *Can. J. Chem.* **1969**, *47*, 3759−3762.

(49) Terry, J. O.; Futrell, J. H. Disproportionation and Combination Reactions of Simple Alkyl Radicals: Methyl, Ethyl, *n*-Propyl, and Isopropyl. *Can. J. Chem.* **1967**, *45*, 2327−2333.

(50) Adachi, H.; Basco, N. A Quantitative Study of Alkyl Radical Reactions by Kinetic Spectroscopy. IV. The Flash-Photolysis of Azopropanes. *Int. J. Chem. Kinet.* **1981**, *13*, 367−384.

(51) Parkes, D. A.; Quinn, C. P. Study of the Spectra and Recombination Kinetics of Alkyl Radicals by Molecular Modulation Spectroscopy. 2. Recombination of Ethyl, Isopropyl, and *tert*-Butyl Radicals at Room Temperature and *tert*-Butyl Radicals between 250 and 450 K. *J. Chem. Soc., Faraday Trans. I* **1976**, *72*, 1952−1971.

(52) Arrowsmith, P.; Kirsch, L. J. Mutual Reaction of Isopropyl Radicals. *J. Chem. Soc., Faraday Trans. I* **1978**, *74*, 3016−3021.

(53) Gibian, M. J.; Corley, R. C. Organic Radical-Radical Reactions, Disproportionation vs Combination. *Chem. Rev.* **1973**, *73*, 441−464.

(54) Nicholas, J. E.; Vaghjiani, G. L. Reaction Probabilities, Cross-Sections, and Threshold Energies in the Reaction of Isotopically Pure H-Atoms and *n*-Butane. *J. Chem. Phys.* **1989**, *91*, 5121−5123.

(55) Jennings, K. R.; Cvetanovic, R. J. Relative Rates of Addition of Hydrogen Atoms to Olefines. *J. Chem. Phys.* **1961**, *35*, 1233−1240.

(56) Yang, K. Free Radical Reactions Initiated by Ionizing Radiations 0.1. Arrhenius Parameters for Reactions of Hydrogen Atoms with Propane, Ethylene and Propylene. *J. Am. Chem. Soc.* **1962**, *84*, 719−721.

(57) Yang, K. Free Radical Reactions Initiated by Ionizing Radiations 3. Paraffin Reactivities in Hydrogen Atom Abstraction Reactions. *J. Phys. Chem.* **1963**, *67*, 562−566.

(58) Mihelcic, D.; Schubert, V.; Hofler, F.; Potzinger, P. Determination of Kinetic Isotope Effects in the Addition Reactions of Hydrogen Atom to Ethylene and Propene with Pulse Radiolysis. *Ber. Bunsen-Ges.* **1975**, *79*, 1230−1239.

(59) Ishikawa, Y.; Yamabe, M.; Noda, A.; Sato, S. Absolute Rate Constants of Reaction of Hydrogen-Atoms with Several Olefins. *Bull. Chem. Soc. Jpn.* **1978**, *51*, 2488−2492.

(60) Oka, K.; Cvetanovic, R. J. Determination of Rates of Hydrogen-Atom Reactions with Alkenes at 298 K by a Double Modulation Technique. *Can. J. Chem.* **1979**, *57*, 777−784.

(61) Harris, G. W.; Pitts, J. N. Absolute Rate Constants and Temperature Dependences for the Gas-Phase Reactions of H-Atoms with Propene and the Butenes in the Temperature-Range 298 to 445 K. *J. Chem. Phys.* **1982**, *77*, 3994−3997.

(62) Watanabe, T.; Kyogoku, T.; Tsunashima, S.; Sato, S.; Nagase, S. Kinetic Isotope Effects in the H + C_3H_6 = C_3H_7 Reaction. *Bull. Chem. Soc. Jpn.* **1982**, *55*, 3720−3723.

(63) Clarke, J. S.; Donahue, N. M.; Kroll, J. H.; Rypkema, H. A.; Anderson, J. G. An Experimental Method for Testing Reactivity Models: A High-Pressure Discharge-Flow Study of H Plus Alkene and Haloalkene Reactions. *J. Phys. Chem. A* **2000**, *104*, 5254−5264.

(64) Bryukov, M. G.; Slagle, I. R.; Knyazev, V. D. Kinetics of Reactions of H Atoms with Ethane and Chlorinated Ethanes. *J. Phys. Chem. A* **2001**, *105*, 6900−6909.

(65) Jones, D.; Morgan, P. A.; Purnell, J. H. Mass-Spectrometric Study of Reactions of Hydrogen Atoms with Ethane. *J. Chem. Soc., Faraday Trans. I* **1977**, *73*, 1311−1318.

(66) Jones, W. E.; Ma, J. L. An Electron-Spin-Resonance Study of the Reactions of Hydrogen Atoms with Halocarbons. *Can. J. Chem.* **1986**, *64*, 2192−2195.

(67) Azatyan, V. V.; Filippov, S. B. Reactions of Atomic Hydrogen and Deuterium with Ethane. *Dokl. Akad. Nauk SSSR* **1969**, *184*, 625.

(68) Kerkeni, B.; Clary, D. C. Ab initio Rate Constants from Hyperspherical Quantum Scattering: Application to $H+C_2H_6$ and $H+CH_3OH$. *J. Chem. Phys.* **2004**, *121*, 6809−6821.

(69) Kerkeni, B.; Clary, D. C. Quantum Dynamics and Kinetics of the Abstraction Reactions by H Atoms of Primary and Secondary Hydrogens in C_3H_8. *Mol. Phys.* **2005**, *103*, 1745−1755.

(70) Klippenstein, S. J.; Georgievskii, Y.; Harding, L. B. Predictive Theory for the Combination Kinetics of Two Alkyl Radicals. *Phys. Chem. Chem. Phys.* **2006**, *8*, 1133−1147.

(71) Sabbe, M. K.; Vandeputte, A. G.; Reyniers, M. F.; Waroquier, M.; Marin, G. B. Modeling the Influence of Resonance Stabilization on the Kinetics of Hydrogen Abstractions. *Phys. Chem. Chem. Phys.* **2010**, *12*, 1278−1298.

(72) Møller, W.; Mozzhukhin, E.; Wagner, H. G. High-Temperature Reactions of CH_3 2. H-Abstraction from alkanes. *Ber. Bunsen-Ges.* **1987**, *91*, 660−666.

(73) Baulch, D. L.; Bowman, C. T.; Cobos, C. J.; Cox, R. A.; Just, T.; Kerr, J. A.; Pilling, M. J.; Stocker, D.; Troe, J.; Tsang, W.; et al. Evaluated Kinetic Data for Combustion Modeling: Supplement II. *J. Phys. Chem. Ref. Data* **2005**, *34*, 757−1397.

(74) Carstensen, H. H.; Dean, A. M. Rate Constant Rules for the Automated Generation of Gas-Phase Reaction Mechanisms. *J. Phys. Chem. A* **2009**, *113*, 367−380.

(75) Peukert, S. L.; Sivaramakrishnan, R.; Michael, J. V. High Temperature Rate Constants for H/D + n-C_4H_{10} and i-C_4H_{10}. *Proc. Combust. Inst.* **2015**, *35*, 171−179.

(76) Takahasi, M.; Cvetanovic, R. J. Secondary Isoptope Effect in Addition of Hydrogen Atoms to Propylene-D_6. *Can. J. Chem.* **1962**, *40*, 1037−1040.

(77) Manion, J. A.; Awan, I. A. Evaluated Kinetics of Terminal and Non-Terminal Addition of Hydrogen Atoms to 1-Alkenes: A Shock Tube Study of H + 1-Butene. *J. Phys. Chem. A* **2015**, *118*, 429−441.